Journal of Marine Research, 68, 767–798, 2010

Journal of
MARINE RESEARCH

Volume 68, Number 6

Sea ice melt and meteoric water distributions in Nares Strait, Baffin Bay, and the Canadian Arctic Archipelago

by Matthew B. Alkire[1,2], Kelly K. Falkner[1], Timothy Boyd[3] and Robie W. Macdonald[4]

ABSTRACT

Sea ice melt (SIM), meteoric water (river runoff + net precipitation), and Pacific seawater contributions to the upper waters of the Canadian Arctic Archipelago (CAA), Nares Strait, and Baffin Bay during late summer 1997 and 2003 are estimated from salinity, $\delta^{18}O$, and nutrient data. Salinity-$\delta^{18}O$ relationships within the study area suggest that the CAA inherits a net sea-ice formation (brine) signal from the Arctic Ocean. Inherited brine complicates the estimation of local contributions from sea ice melt and glacial runoff, especially where a significant component of the surface water derives from Arctic outflow. Our data are characterized by two linear relationships between salinity and $\delta^{18}O$, reflecting: (1) the mixing of deeper Atlantic seawater with brine-enriched halocline water of shelf origin and (2) mixing of halocline water with shallower waters freshened by meteoric water and local SIM. Inventories of Pacific water, meteoric water, net SIM, and local SIM were computed over the upper 150 m of the water column. Positive local SIM fractions were ubiquitous during late summer, with the largest inventories ($>$1 m) found on the eastern sides of Baffin Bay, Kennedy Channel, and Davis Strait. In the CAA and Baffin Bay, freshwater inventories were dominated by contributions from meteoric and Pacific water, with little input from local SIM. In Smith Sound, where comparable data were collected in 1997 and 2003, meteoric water inventories of 8–10 m were similar for both years, whereas the Pacific water inventory was substantially lower in 2003 ($<$80 m) than in 1997 ($>$100 m), implying that the export of meteoric water from the Arctic Ocean is decoupled from Pacific water outflow.

1. College of Oceanic and Atmospheric Sciences, Oregon State University, Corvallis, Oregon, 97331, U.S.A.
2. Present address: Applied Physics Laboratory, University of Washington, Seattle, Washington, 98105, U.S.A. ***email: malkire@apl.washington.edu***
3. Scottish Association for Marine Science, Scottish Marine Institute, Oban, Argyll PA37 1QA, Scotland.
4. Institute of Ocean Sciences, Fisheries and Oceans Canada, Sidney, British Columbia V8L 4B2, Canada.

1. Introduction

The Canadian Arctic Archipelago (CAA), a major conduit for Arctic Ocean outflow, accounts for approximately half of the freshwater exported from the Arctic to the North Atlantic (Serreze *et al.,* 2006). Freshwater moving through the Arctic Ocean to the CAA and Baffin Bay has three main sources: *meteoric water* (MW), *sea ice meltwater* (SIM), and *Pacific water* (PW). Meteoric water, which is water that has undergone distillation and transport in the atmosphere, includes river inflow to the Arctic Ocean from the extensive drainage basins of the Eurasian and North American continents and direct precipitation on the ocean. Large volumes of older MW have been stored in glaciers. Many of these, including small glaciers in the CAA as well as those of the Greenland icecap, are currently undergoing accelerated ablation and are thus providing increasing inflows of MW to the ocean (Luthcke *et al.,* 2006; Rignot *et al.,* 2008; Velicogna, 2009; Dyurgerov *et al.,* 2010).

Sea ice meltwater is brackish. The bulk salinity of sea ice is 4–20 and decreases with age, although most of the salt is initially rejected during its formation from seawater (Weeks and Ackley, 1986). Sea ice withdraws freshwater from the ocean during ice formation (negative SIM) and adds freshwater back to the ocean during melt (positive SIM). As these two processes are decoupled in time and space, sea ice formation and melting have the capacity to affect freshwater distribution in the ocean even though the net sea ice cycle must balance its salt. Pacific water entering the Arctic Ocean through the Bering Strait provides a third source of freshwater. Freshwater content in the ocean is always defined relative to a reference salinity. In the Arctic Ocean, the salinity of Atlantic seawater (S∼34.87) is usually used as the reference value (Serreze *et al.,* 2006; Aagaard and Carmack, 1989), and PW thus represents a source of freshwater to the Arctic Ocean because it contains MW accumulated from river inflow from North America and net precipitation in the Pacific Ocean and Bering Sea.

Variability in freshwater flux through the CAA and Baffin Bay may have broad downstream consequences. The freshwater passing through Baffin Bay, including that tied up in sea ice, is delivered to the Labrador Sea where North Atlantic Deep Water is formed (Aagaard and Carmack, 1989). Variability in the quantity of freshwater exported from the CAA will, therefore, contribute to variability in stratification at sites of convective overturning, with the potential to impact this key northern limb of global ocean overturning circulation (Aagaard and Carmack, 1989; Tang *et al.,* 2004; Jungclaus *et al.,* 2006; Stouffer *et al.,* 2006).

The specific impacts of an increase in the freshwater flux from the Arctic are still under debate (e.g., Myers, 2005; Gerdes *et al.,* 2008), however freshening of North Atlantic surface waters via water exported from the Arctic Ocean has the potential to decrease the aragonite saturation state (Yamamoto-Kawai *et al.,* 2009; Steinacher *et al.,* 2009; Azetsu-Scott *et al.,* 2010; Shadwick *et al.,* 2011), thus enhancing the sensitivity of this region to ocean acidification by anthropogenic CO_2. Variability in the flux through Baffin Bay of freshwater of Arctic Ocean origin is thought to be related to variability in Arctic Ocean freshwater inputs, storage and export resulting from large-scale circulation and atmo-

spheric forcing patterns (Proshutinsky *et al.,* 2002; Steele *et al.,* 2004; Falck *et al.,* 2005; Sutherland *et al.,* 2009; Aksenov *et al.,* 2010; Jahn *et al.,* 2010).

Hence it is important to gain an understanding of the relative importance of the processes contributing to variability in freshwater distributions and fluxes in the Baffin Bay region. In this paper, we quantify the Pacific water, sea ice melt, and meteoric water components of the freshwater distributions in Baffin Bay, Nares Strait, and the CAA using nutrient relationships, oxygen isotope ratios ($\delta^{18}O$), and salinity data to account for both the inherited and local freshwater signals. We also discuss the complications that water properties inherited from the Arctic Ocean present in identifying and quantifying the contribution of local glacial ice melt to the upper ocean.

2. Background

a. Hydrographic setting

Transport of water through the CAA is limited by relatively shallow sills in numerous straits and sounds along the various channels between the Arctic Ocean and Baffin Bay. En route to Baffin Bay, Arctic surface water must pass through Nares Strait (sill depth ~220 m), Cardigan Strait/Hell Gate (~180/125 m), or Barrow Strait (~125 m) to reach Smith, Jones, and Lancaster sounds, respectively (Fig. 1; Melling *et al.,* 2008). A small fraction of Arctic water passing through the CAA is diverted to the Hudson Bay system via Fury and Hecla (~170 m) straits (Straneo and Saucier, 2008; Serreze *et al.,* 2006; Prinsenberg and Hamilton, 2005; Drinkwater *et al.,* 1988). This water entrains more than 700 km^3 yr^{-1} of runoff (Straneo and Saucier, 2008) before it eventually exits into southwestern Baffin Bay via Hudson Strait (~200 m). Exchange with waters of the Labrador Sea also occurs at this southern boundary via Davis Strait (~650 m).

Two major water types dominate the upper 500 m of Baffin Bay: warm and saline ($33.7 \leq S \leq 34.55$) West Greenland Intermediate Water (WGIW) entering via the eastern channel of Davis Strait, and cold, relatively fresh ($S < 33.7$) water originating largely in the Arctic Ocean (Tang *et al.,* 2004). The seawater component of Arctic Ocean water entering Baffin Bay through the CAA is predominately of Pacific origin, but Atlantic-derived waters are also present in proportions that increase with depth and in the northern part of the bay (Munchow *et al.,* 2007; Falkner *et al.,* in preparation). The upper 200 m of the water column is additionally imprinted by local contributions of SIM and MW, but these two freshwater components may also be advected into the region from the Arctic Ocean along with the seawater.

The large-scale circulation in Baffin Bay is generally cyclonic (Tang *et al.,* 2004). Cold, relatively fresh waters of Arctic origin are transported in the Baffin Current, which starts near the entrance to Smith Sound and flows southward along western Baffin Bay, offshore of the 500 m isobath, to western Davis Strait. Along its southward trajectory, the Baffin Current exchanges water with the flows through Jones Sound, Lancaster Sound, and Hudson Strait. Warm and relatively saline waters of Atlantic origin enter Baffin Bay at

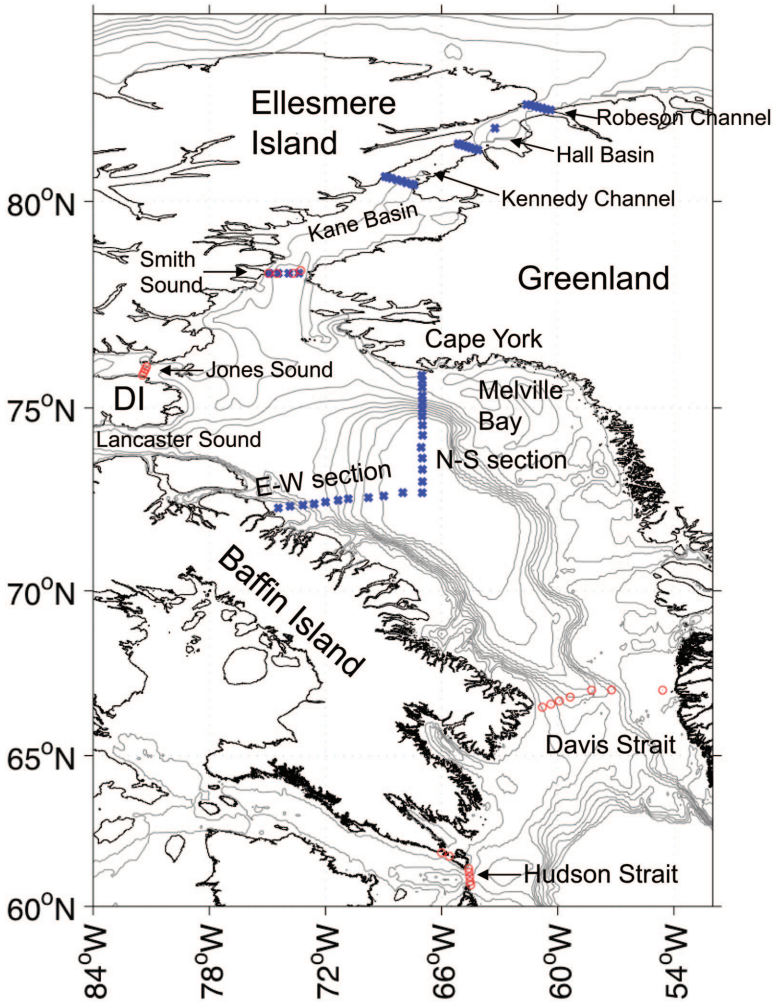

Figure 1. Map of study area. Stations occupied during 1997 and 2003 are plotted as circles and x's, respectively. Nares Strait consists of (from north to south) the Robeson Channel (separating Lincoln Sea and Hall Basin), Kennedy Channel (separating Hall Basin and Kane Basin), and Smith Sound (separating Kane Basin and Baffin Bay). Note the acronym DI stands for Devon Island. Isobaths range from 500 to 2500 meters (500 meter intervals). Coastline data obtained from the NOAA National Geophysical Data Center Coastline Extractor (http://rimmer.ngdc.noaa.gov/mgg/coast/getcoast.html). Bathymetry data obtained from the TerrainBase, Global 5-Minute Ocean Depth and Land Elevation data set (http://dss.ucar.edu/datasets/ds759.2/).

eastern Davis Strait via the northward flowing West Greenland Current (WGC). Branches of this current turn westward at Melville Bay and south of Cape York and eventually re-circulate in western Davis Strait (Tang *et al.,* 2004).

The remaining flow continues along the Greenland shelf and slope as far north as eastern

Table 1. Endmember definitions for water type analyses.

Water type	Salinity	$\delta^{18}O$ (‰)	Uncertainty*
Sea-ice melt	6 ± 2	0.05 ± 2	0.03
Pacific seawater	32.5 ± 1	-0.8 ± 0.3	0.14
Atlantic seawater	34.87 ± 0.03	0.24 ± 0.05	0.14
Meteoric Water	0	-18.8 ± 3**	0.03

*Maximum uncertainty in water type fractions derived from varying salinity and $\delta^{18}O$ definitions within limits of variability specified. Note larger uncertainty in Pacific and Atlantic fractions is due to inherent uncertainty in the dissolved inorganic nitrogen:phosphate ratios defined (Taylor *et al.,* 2003).

**A $\delta^{18}O$ value of -14‰ was assigned for the meteoric water endmember in the water type calculations for Hudson Strait (Granskog *et al.,* 2009).

Smith Sound, but the majority of this water likely re-circulates in Kane Basin and returns southward (Tang *et al.,* 2004; Munchow *et al.,* 2007). Although the CAA supports a net flow out of the Arctic Ocean, the widths of some channels permit complex interior circulations that include reverse flow, especially along the northern sides of the channels (Coote and Jones, 1982; McLaughlin *et al.,* 2006). Water flowing westward from Baffin Bay into the northern sides of Jones and Lancaster sounds mixes with CAA throughflow before returning to Baffin Bay on the southern sides of the channels (Fissel *et al.,* 1988).

b. On the use of oxygen isotopes to quantify water types in high latitude waters

The oxygen isotope composition of water is typically expressed relative to Vienna Mean Standard Ocean Water (VSMOW) as:

$$\delta^{18}O = \{(R_{sample} - R_{VSMOW})/R_{VSMOW}\} \times 1000 \quad (1)$$

where $R = {}^{18}O/{}^{16}O$. Both equilibrium thermodynamic and kinetic effects favor the accumulation of lighter isotopes of water in the vapor phase and heavier isotopes in the liquid phase (Craig and Gordon, 1964). Repeated evaporation and precipitation cycles thus cause northern latitude meteoric waters to be highly depleted in ^{18}O relative to seawater (see Table 1). Conservative mixing between reservoirs of meteoric water of uniform $\delta^{18}O$ composition and a seawater endmember produces a linear relationship between salinity and $\delta^{18}O$ (Paren and Potter, 1984). Extrapolation to zero salinity of such linear fits can be used to infer the $\delta^{18}O$ of the MW and thus its source (e.g., Redfield and Friedman, 1969; Tan and Strain, 1980; Bedard *et al.,* 1981; Ostlund and Hut, 1984; Kipphut, 1990; Tan and Strain, 1996; Cooper *et al.,* 1997).

In polar environments, however, sea ice melt/formation processes also affect the freshwater composition such that the salinity-$\delta^{18}O$ relationship need no longer be linear. When sea-ice forms, heavier isotopes are preferentially incorporated into the solid phase to a small extent, with a fractionation factor of $+1.9 - 2.3$‰ (Macdonald *et al.,* 1995). Simultaneously, most of the salt is excluded during the initial formation of sea ice, which

continues to lose salt through brine drainage as the ice ages (Weeks and Ackley, 1986). The initial salinity of newly formed sea ice can be as high as 10 or 20; however, the salinity typically decreases to 4–6 within a year, and multi-year ice can have even lower salinities (Weeks and Ackley, 1986).

To compute fractional contributions of meteoric water (MW), sea ice meltwater (SIM), and seawater (SW) in any given sample, conservation equations for salinity, $\delta^{18}O$, and mass (or volume) can be used provided the endmember characteristics are known (e.g., Ostlund and Hut, 1984; Schlosser *et al.,* 1994; Bauch *et al.,* 1995; Yamamoto-Kawai *et al.,* 2005; 2008; Alkire *et al.,* 2007):

$$S_{SIM} \times f_{SIM} + S_{MW} \times f_{MW} + S_{SW} \times f_{SW} = S_{observed} \tag{2}$$

$$\delta^{18}O_{SIM} \times f_{SIM} + \delta^{18}O_{MW} \times f_{MW} + \delta^{18}O_{SW} \times f_{SW} = \delta^{18}O_{observed} \tag{3}$$

$$f_{SIM} + f_{MW} + f_{SW} = 1 \tag{4}$$

where f is the fraction of mass (or volume) contributed by a given component. Note that net sea-ice formation (formation exceeds melting) will generate a negative SIM fraction ($f_{SIM} < 0$).

3. Methods

a. Sampling and analyses

Water sampling was conducted along transects crossing several straits bounding Baffin Bay during Legs 1–3 of the US-Canadian Joint Ocean Ice Studies (JOIS), aboard the CCGS *Louis S. St. Laurent* between August 1 and September 2, 1997 (Fig. 1, circles). Water sampling was also conducted on several transects across Nares Strait and Baffin Bay as part of the Canadian Archipelago Throughflow Study (CATS), aboard the USGCS *Healy* between July 26 and August 11, 2003 (Fig. 1, x's). In 1997, data were acquired on transects at Hudson and Davis straits and across the entrances to Smith and Jones sounds in 1997. In 2003, data were acquired on transects across Robeson Channel, the northern and southern ends of Kennedy Channel, Smith Sound, and central Baffin Bay. The full data sets are available online via the Institute of Ocean Sciences, Department of Fisheries and Oceans, Canada (1997 data; http://www.dfo-mpo.gc.ca/libraries-bibliotheques/data-stat-hydro-eng.htm) and the National Snow and Ice Data Center (2003 data; http://nsidc.org/data/index.html).

Conductivity-temperature-depth (CTD) data and seawater samples were collected using a rosette system during the cruises. In 1997, the CTD (Falmouth Scientific, Inc.) was deployed together with 23 ten-liter PVC bottles developed by Brooke Ocean Technology. In 2003, a Sea-Bird Electronics, Inc. SBE9*plus* CTD outfitted with an SBE43 dissolved oxygen sensor was deployed in the rosette along with 24 twelve-liter Ocean Test Equipment PVC bottles.

Bottle salinities were determined at sea after a 12-hour equilibration to a controlled room

temperature using a model 8400A Guideline Autosal salinometer. Precision, based on sample replicates, is estimated to be ±0.003 in 1997 and ±0.001 in 2003. In 1997, concentrations of nutrients NO_3^-, NO_2^-, NH_4^+, PO_4^{3-}, and Si were determined at sea via a Technicon Autoanalyser II following published procedures (Armstrong *et al.,* 1967; Bernhardt and Wilhelms, 1967). Precision is estimated to be ±1% based on sample replicates. In 2003, nutrient concentrations were determined at sea with similar precision using a hybrid Alpkem RFA 300 and Technicon AA-II (AutoAnalyzer II)–based system with the JGOFS/WOCE suggested protocols (Gordon *et al.,* 1994). The Si, $NO_3^- + NO_2^-$, and NO_2^- channels were RFA-based, and the PO_4^{3-} and NH_4^+ channels were AA-II-based. Oxygen isotopes were analyzed by the CO_2 equilibration method on the COAS Finnegan Mat 251 mass spectrometer at Oregon State University. Results are reported in del units relative to VSMOW. Precision (1σ) is estimated to be ±0.03‰ based on sample replicates.

b. Water component analysis

Salinity and isotope endmember characteristics (Table 1) were assigned as follows. The sea ice meltwater endmember characteristics are representative of first-year ice values typically observed in the CAA and Baffin Bay (Strain and Tan, 1993; Rigor and Wallace, 2004). The meteoric water endmember $\delta^{18}O$ value is the volumetric (flow-weighted) average of Arctic river runoff (Cooper *et al.,* 2008), which is the main source of meteoric water entering Baffin Bay from the Arctic Ocean, and is comparable to the isotopic composition of local meteoric water (i.e., Baffin Bay precipitation and runoff; Tan and Strain, 1980, 1996; Ostlund and Hut, 1984). The meteoric water endmember was revised to a heavier isotopic value (−14‰) only for Hudson Strait, as this better represents local inputs to Hudson Bay (Granskog *et al.,* 2009).

Natural variability in the salinity and $\delta^{18}O$ characteristics of meteoric water and sea ice meltwater leads to uncertainty in the fractional contributions that result from solving the coupled set of equations (2–4). Propagating the extreme values of the range of observed endmember variability results in maximum variations of 3% in component fractional composition. For example, the use of SIM endmember values more typical of aged ice ($S = 4$, $\delta^{18}O = -2$‰) would yield solutions for meteoric water fractions only 1% higher than those computed using the assigned endmember values (Table 1). Thus, the water type analysis is robust to typical sea ice melt and meteoric water variability within the limits of uncertainty shown in Table 1.

Pacific and Atlantic water endmember values (Table 1) represent the inflows to the Arctic Ocean via Bering and Fram Straits, respectively (Yamamoto-Kawai *et al.,* 2008). This choice is unambiguous for Pacific water, which can be traced back to a source at Bering Strait. Atlantic water, however, enters the Baffin Bay study region both through the CAA passages and via Davis Strait. The salinity-$\delta^{18}O$ relationship for salinities greater than 33 and depths between 150 and 500 meters, where the influence from Pacific water and both Baffin Bay Deep and Baffin Bay Bottom waters are negligible, is roughly linear (see Table 2). A linear regression of these data yields the same value of $\delta^{18}O = 0.24 \pm$

Table 2. Coefficients from simple linear regression of salinity and Δ ($= \delta^{18}O \times (1 - S/1000)$, Paren and Potter, 1984) for sections occupied in 1997 and 2003. Data included in the regression were collected between 150 and 500 meters depth to ensure minimal influence from local sea ice meltwater. Lower and Upper Slopes and Intercepts represent bounds on these parameters computed from the 95% confidence intervals of the linear regression. The correlation coefficient (R) and number of data points (N) utilized in the regression are also tabulated. $\delta^{18}O_{AW}$ is the value resulting from extrapolation of the linear regression to the AW salinity of 34.87.

Section	Slope	Lower slope (95% CI)	Upper slope (95% CI)	Intercept (‰)	Lower intercept (95% CI)	Upper intercept (95% CI)	R	N	$\delta^{18}O_{AW}$ (‰)
2003									
Robeson Channel	0.97	0.63	1.31	−33.5	−45.3	−21.8	0.8181	20	0.28
N. Kennedy Channel	1.07	0.92	1.21	−36.9	−41.7	−32.0	0.9704	18	0.26
S. Kennedy Channel	0.95	0.85	1.05	−33.0	−36.5	−29.5	0.9832	16	0.22
Smith Sound	0.93	0.84	1.01	−32.0	−35.0	−29.1	0.9837	19	0.22
N–S Baffin Bay	0.99	0.87	1.10	−34.1	−38.0	−30.3	0.9717	22	0.24
E–W Baffin Bay	1.14	1.09	1.19	−39.2	−40.9	−37.6	0.9900	45	0.34
1997									
Smith Sound	0.77	0.66	0.88	−26.8	−30.6	−23.0	0.9446	26	0.02
Jones Sound	0.94	0.82	1.06	−32.6	−36.7	−28.6	0.9595	25	0.18
Hudson Strait	0.77	0.70	0.84	−26.6	−29.0	−24.3	0.9627	42	0.21
Davis Strait	1.00	0.93	1.07	−34.4	−36.8	−32.1	0.9809	35	0.27

1.86‰ as Yamamoto-Kawai *et al.* (2008) found for the canonical Atlantic water salinity of 34.87 and which we use throughout for a single Atlantic water endmember value.

Because the decomposition defined by Eqs. 2–4 is described in terms of a general seawater component, the proportion of Atlantic and Pacific seawater must first be determined for each sample. The ratios of concentrations of dissolved inorganic nitrogen ($DIN = NO_3^- + NO_2^- + NH_4^+$) to phosphate were used to distinguish between Pacific and Atlantic seawater contributions within water samples, following the methodology developed by Jones *et al.* (1998) (see also, Taylor *et al.,* 2003; Alkire *et al.,* 2007; and Yamamoto-Kawai *et al.,* 2008). Pacific and Atlantic seawater proportions were then used to calculate salinity and $\delta^{18}O$ characteristics of a combined seawater endmember for each sample in accordance with Table 1. Eqs. 2–4 were solved simultaneously to determine the fractional contributions of the combined seawater, meteoric, and sea ice meltwater components to each water sample. The net Pacific and Atlantic contributions for each sample were then obtained by multiplying the resultant seawater endmember fraction by the proportions of Pacific and Atlantic waters contributing to the sample-specific combined seawater endmember.

4. Estimating the local sea ice melt component

a. Interpretation of salinity-$\delta^{18}O$ extrapolations

Tan and Strain (1980) assumed the near-surface waters of Baffin Bay were a mixture of seawater and meteoric water, and they defined an upper ocean reference state by the least

squares linear fit of $\delta^{18}O$ to salinity over the depth range of 5 m to 150 m. Differences between measured isotope values and those predicted by the regression line were attributed to the addition of seasonal/local sea ice meltwater. Strain and Tan (1993) later revisited the Baffin Bay $\delta^{18}O$ data to address variability in the slopes of their reference regression lines among different profiles. Specifically, they sought to address the consequent problem that the extrapolations of their regression lines to "apparent" freshwater ($S = 0$) endmember $\delta^{18}O$ values were variable (ranging from -33.1 to $-45.1‰$ in Baffin Bay) and did not correspond to the dominant meteoric input to Baffin Bay. Using a box model, they demonstrated that the partitioning of meltwater and brine could alter the shape of the salinity-$\delta^{18}O$ relationship during the melt and freeze seasons and thus significantly alter both the slopes and intercepts of apparent mixing lines.

The extrapolated endmember values for the apparent freshwater ($-40 \leq \delta^{18}O \leq -26‰$, see Table 2) in this study, like those found by Tan and Strain (1980), are significantly different from average Arctic meteoric water ($-18.8‰$). High altitude precipitation, such as that atop the ice sheets of Greenland and the islands of the Canadian Archipelago, has a typical $\delta^{18}O$ range between -20 and $-30‰$, and some estimates as low as $-40‰$ have been reported (Dansgaard and Tauber, 1969; Koerner and Russell, 1979; Bedard *et al.,* 1981). Thus, glacial meltwater can be a potential source of such highly negative $\delta^{18}O$ values. However, combined estimates of glacial meltwater flux from the entire Greenland landmass in 2000–2004 range from 160 to 230 $km^3\ yr^{-1}$ (Luthcke *et al.,* 2006; Rignot *et al.,* 2008). This flux is small compared to the current estimated total freshwater flux entering Baffin Bay through CAA passages (3200 $km^3\ yr^{-1}$; Serreze *et al.,* 2006). It is likely, therefore, that the highly-negative $\delta^{18}O$ values extrapolated in this study are an artifact of mixing seawater with sub-surface water enriched by brine during sea ice formation, in agreement with the conclusions of Strain and Tan (1993).

If sea ice formed during winter circulates together with the water containing its rejected brine and the SIM subsequently re-mixes with that water, the system would return to a zero ice formation tracer signal ($f_{SIM} = 0$). However, differential transport of water and sea ice, commonly encountered at the perimeter of the Arctic Ocean, can separate the processes of ice formation and melt (Pfirman *et al.,* 2004). Brine and SIM can also be separated by penetrative convection such that dense brine sinks into or below the halocline while buoyant SIM accumulates at the surface where it cannot mix with the brine (Macdonald, 2000).

Tan and Strain (1996) applied the box model developed by Strain and Tan (1993) to salinity and $\delta^{18}O$ data from Foxe Basin and Hudson Bay to determine a reference mixing line against which seasonal SIM contributions could be calculated. This reference line represents the salinity-$\delta^{18}O$ relationship prior to the start of the melt season. It therefore "subtracts" the effect of net ice formation on the upper layers of the water column, so that sea ice melting that summer can be detected despite the history of predominant ice formation (brine injection) on the waters sampled. Application of Eqs. 2–4 (see Section 2b) yields fractional contributions representing the net effect sea ice melt–formation, integrated over the age (time since subduction out of the surface layer) of the water.

Seasonal/local sea ice melt typically is not large enough to produce a positive fraction in such a reference frame, only a less negative one. Thus, the box model changes the reference frame to be more suitable to detect local SIM. Here, we attempt to improve upon the methods of Tan and Strain (1996) by re-defining the reference line against which local SIM contributions are calculated.

b. Export of net ice formation (brine) from the Arctic Ocean

Where does water found in Baffin Bay acquire this enriched brine signature? Although we cannot completely discount contributions by local ice formation within Baffin Bay, examination of regional data suggests that brine-enriched waters are delivered from the Arctic Ocean. Bauch *et al.* (2009) reported brine-enriched bottom water on the southern Laptev shelf, presumably produced via net ice formation in the persistent polynya that occurs there. Entrainment of this shelf bottom water into the Arctic Ocean halocline was observed at the Laptev shelf break where it mixes with Atlantic water. Mixing also occurred at shallower depths with lower-salinity shelf waters, influenced by Lena River input, generating a separate trend in salinity-$\delta^{18}O$ space.

Examination of Arctic Ocean data from 1958–2001 in the Seawater Oxygen-18 Database (Schmidt *et al.,* 1999) reveals that salinity-$\delta^{18}O$ data from the various regions of the deep basins and over the Arctic shelves often differ significantly from the meteoric-Atlantic water mixing trend (Fig. 4). Data from the Barents Sea plot mostly above the meteoric-Atlantic water mixing line, indicating net freshening by SIM (Fig. 4a). Meteoric water influence is more pronounced in the Kara (Fig. 4b), Laptev (Fig. 4c), East Siberian (Fig. 4d), and Chukchi (Fig. 4g) Seas where much of the data conform to a meteoric-Atlantic water mixing trend. Even in these regions, where there is a pervasive input of MW, departures below the mixing line indicate a significant input of brine between salinities 31.0 and 33.5. Data from the Beaufort Sea (Fig. 4h) and the Eurasian (Fig. 4e) and Canadian (Fig. 4f) basins all indicate significant brine input throughout the salinity range 30–34.2, which can only occur where salt rejected by ice formation sinks below the depth where seasonal mixing can re-unite brine and SIM. The distribution of data in the CAA and Baffin Bay (Figs. 2–3, 4i) likewise show an imprint of brine throughout this salinity range.

The strong net ice formation signal observed in the central basins of the Arctic Ocean over salinities 30 to 34.2 is advected downstream into Baffin Bay through the CAA and Nares Strait. Circulation patterns of the upper layers of the Arctic Ocean suggest that Canadian Basin waters are more likely to supply Lancaster and Jones sounds via the CAA, while both the Canadian and Eurasian basins supply Nares Strait and Smith Sound (e.g., Rudels, 1986; Steele *et al.,* 2004). Previous work suggests that the upper 100 meters of Robeson Channel resemble waters from either the Eurasian (Muench, 1971) or Canadian (Melling *et al.,* 1984) basins while waters below 200 meters have characteristics similar to the Canadian Basin (Muench, 1971). CATS hydrographic tracer data from August 2003 (unpublished) indicate a blend of Canadian and Eurasian Basin waters in Robeson Channel. The brine contained in this flow therefore may originate in sea ice formation processes distributed along Arctic shelves, and the signature

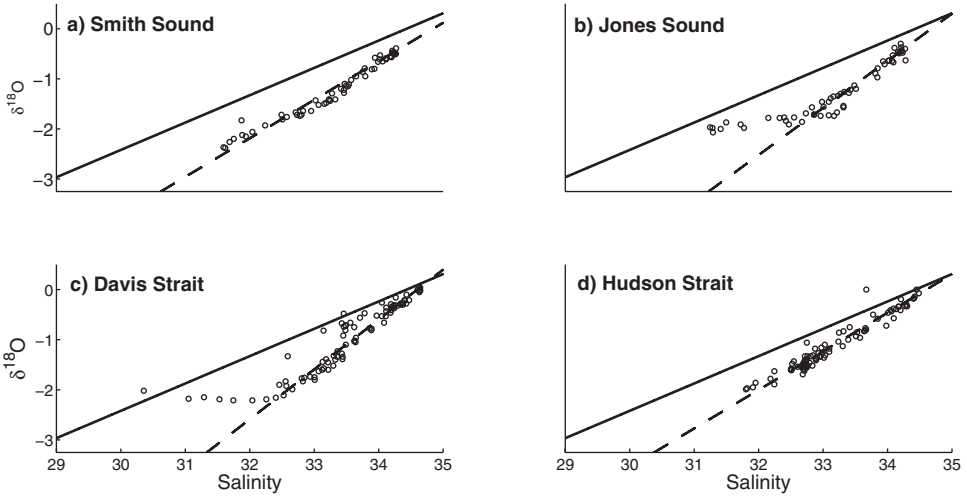

Figure 2. Salinity vs. $\delta^{18}O$ plots for sections occupied during summer 1997. Included in each plot are the Atlantic-halocline water mixing lines (dashed), derived from linear regressions of data collected between 150 and 500 meters, and the typical meteoric-Atlantic water mixing line (solid) specified for the Arctic interior ($\delta^{18}O = 0.546 \times S - 18.8‰$).

persists throughout advection to Baffin Bay because it remains below surface layers subject to inputs of seasonal ice melt and mixing.

c. Two-layer model for calculation of local sea ice melt

A CATS station from Smith Sound in August 2003 (Fig. 5) illustrates the way in which the data distribution, relative to salinity-$\delta^{18}O$ mixing lines, can be used to infer the relative

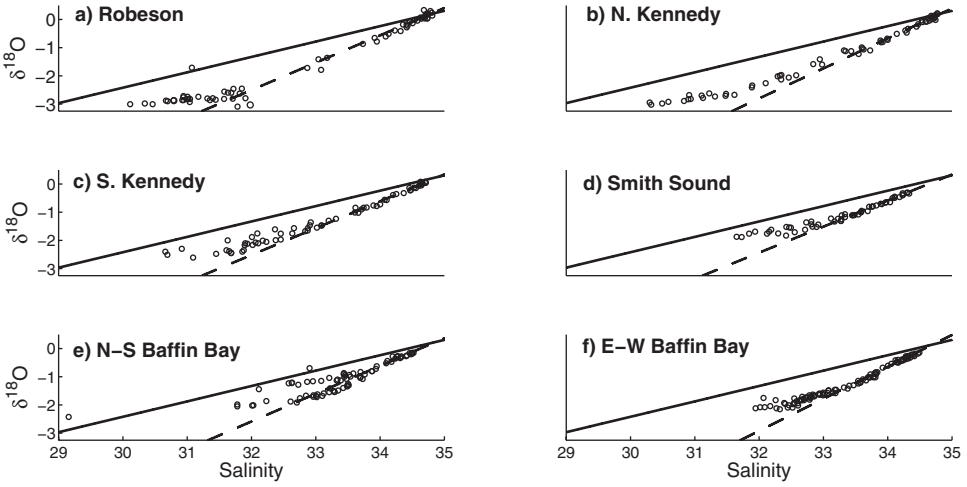

Figure 3. Same as for Figure 2 but for sections occupied during summer 2003.

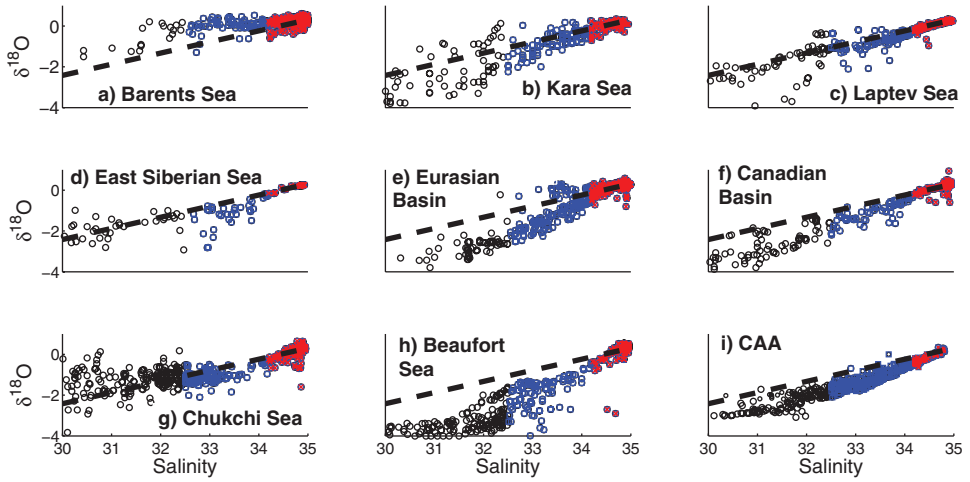

Figure 4. Plots of salinity versus $\delta^{18}O$ for separate regions from the Oxygen-18 Database (Schmidt *et al.,* 1999). Data are color-coded according to salinity range: black circles (salinity > 30), blue squares (salinity > 32.5), and red diamonds (salinity > 34.2). Also included in each diagram is the average meteoric-Atlantic water mixing line, departures from which are typically used to identify the presence of sea ice meltwater or brine. Departures above (below) indicate the presence of meltwater (brine).

importance of local processes. In this example, following the work of Bauch *et al.* (2009), one possible S-$\delta^{18}O$ relationship (i.e., linear mixing) would result from mixing Atlantic water with average Arctic meteoric water. Another linear relationship would result from mixing between Atlantic water and brine-enriched halocline water. The salinity and $\delta^{18}O$ values of the halocline water endmember are expected to vary depending on the intensity of ice formation and depth of the shelf of origin (Bauch *et al.,* 2009). For salinities < 33, the CATS data (Fig. 5) lie in a band between the two main mixing lines, implying variable contributions from brine-enriched halocline water and typical meteoric water.

To quantify the influence of local sea ice formation/melt processes, we assume Baffin Bay to be a two-layer system, in which sea ice melt and meteoric water are confined to mix only within the upper layer and the lower layer is a mix between Atlantic-origin and brine-enriched shelf waters. We take separate linear regressions of data between 150 and 500 meters for each section (Table 2) to produce an Atlantic-halocline water mixing line. Local SIM may be neglected because little, if any, can penetrate to these depths (Muench, 1971; Tan and Strain, 1980; Wallace, 1985). Supporting this assumption, the extrapolation of such regression lines to Atlantic water salinity ($S = 34.87$) yields $\delta^{18}O$ values (Table 2) consistent with the Atlantic water endmember $\delta^{18}O$ value shown in Table 1 (0.24‰), with the exception of the 1997 section across Smith Sound.

Having derived a reference mixing line between deeper Atlantic water and halocline water for each section (see Fig. 1), mixing lines between the halocline water and average

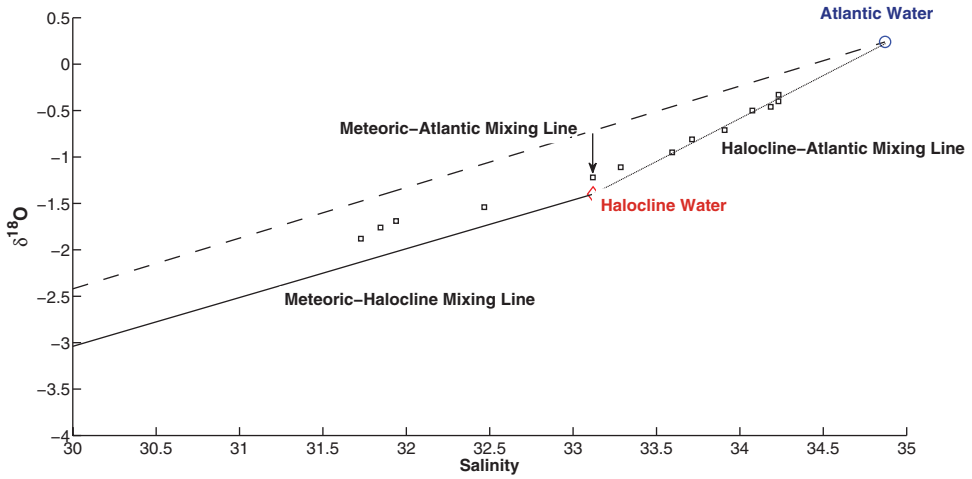

Figure 5. Schematic of mixing in a two-layer system for an example station occupied in Smith Sound during 2003. Brine-enriched halocline water advected from the Arctic interior is represented as a separate water type denoted by the diamond. Mixing between meteoric water (S = 0, $\delta^{18}O = -18.8‰$) and this Arctic halocline water will produce water that falls on the solid line. Samples containing local sea ice melt or brine will plot above or below this line, respectively. Deeper waters having no local sea ice melt influence can be described relative to the Arctic inflow, as mixing between a seawater endmember (e.g., Atlantic water, denoted by the circle) and either meteoric water (dashed line) or halocline water (dotted line). The salinity and $\delta^{18}O$ values of the halocline water endmember are assigned based on the maximum deviation of the measurements from the meteoric-Atlantic water mixing line, denoted by the arrow (see Section 4c for details).

meteoric water are then derived separately for each station. This requires the selection of endmember $\delta^{18}O$ and S values for the halocline water, which is assumed to lie somewhere along the halocline-Atlantic water mixing line for each section (Fig. 5). Graphically, the three endmembers (meteoric, halocline, and Atlantic waters) can be considered as vertices of a triangle in salinity-$\delta^{18}O$ space with the halocline water endmember located farthest from the side of the triangle connecting the remaining vertices (i.e., the meteoric-Atlantic water mixing line). Thus, the halocline water endmember salinity value (Fig 5; Table 3) for each station was selected as the salinity data value associated with the largest negative $\delta^{18}O$ deviation from the meteoric-Atlantic mixing line. The halocline endmember $\delta^{18}O$ value was then computed as the halocline-Atlantic mixing line value at that salinity.

The conservation equations (2–4) used to compute fractional contributions of meteoric water, seawater, and net sea ice meltwater were adapted to calculate fractions of local sea ice meltwater. The steps outlined in Section 2b were repeated here, except the salinity and $\delta^{18}O$ endmember values characterizing halocline water were used in place of the seawater endmember (SW in equations 2–4). Endmember values for meteoric water (MW) and sea ice meltwater (SIM) remained the same (Table 1). Samples with $\delta^{18}O$ values above (below) the meteoric-halocline mixing line result in positive (negative) local sea ice melt

Table 3. Estimated salinity and $\delta^{18}O$ of halocline water for each station occupied during *Healy* 2003 and *Louis St. Laurent* (LSSL) 1997 cruises. Halocline salinity and $\delta^{18}O$ at stations BNS 6, BNS 9–10, and D9 were taken from the mean of stations BNS 2, 4, and 7; BNS 11–14; and station D6, respectively due to too few data points ($n < 5$) to comprise a reliable linear regression. Inventories (in meters) of local sea ice meltwater (LSIM) are reported in the last column. Details on the associated calculations are given in Section 4c.

Cruise	Station	Latitude	Longitude	S_{HW}	$\delta^{18}O_{HW}$ (‰)	LSIM (m)
Healy03	B1	72.753	−67.025	33.18	−1.58	0.5
Healy03	BEW2	72.753	−68.006	33.19	−1.57	0.2
Healy03	BEW3	72.664	−68.993	32.80	−2.01	0.8
Healy03	BEW4	72.619	−69.779	32.52	−2.33	0.6
Healy03	BEW5	72.586	−70.826	32.85	−1.95	0.8
Healy03	BEW6	72.543	−71.354	32.53	−2.31	0.3
Healy03	BEW7	72.498	−72.003	32.70	−2.12	0.9
Healy03	BEW8	72.449	−72.580	32.27	−2.61	0.4
Healy03	BEW9	72.412	−73.170	32.60	−2.24	0.7
Healy03	BEW10	72.384	−73.836	32.46	−2.39	1.4
Healy03	BEW11	72.336	−74.441	32.58	−2.26	1.2
Healy03	BNS2	73.054	−66.996	32.71	−1.89	0.0
Healy03	BNS3	73.382	−66.996	33.02	−1.59	0.0
Healy03	BNS4	73.682	−67.002	33.29	−1.31	0.2
Healy03	BNS5	73.969	−67.061	-	-	-
Healy03	BNS6	74.288	−66.986	33.03	−1.57	0.0
Healy03	BNS7	74.553	−66.990	33.10	−1.50	0.0
Healy03	BNS8	74.786	−67.001	-	-	-
Healy03	BNS9	74.971	−67.001	33.46	−1.15	0.2
Healy03	BNS10	75.135	−66.996	33.46	−1.15	0.5
Healy03	BNS11	75.312	−67.002	33.54	−1.07	0.6
Healy03	BNS12	75.533	−67.001	33.52	−1.09	0.5
Healy03	BNS13	75.701	−67.005	33.46	−1.15	0.8
Healy03	BNS14	75.835	−67.027	33.33	−1.28	1.8
Healy03	S1	78.332	−72.914	33.49	−1.06	0.2
Healy03	S2	78.339	−73.376	33.12	−1.40	0.8
Healy03	S3	78.332	−73.890	33.27	−1.26	0.3
Healy03	S4	78.333	−74.437	33.28	−1.26	0.3
Healy03	S5	78.332	−74.898	32.42	−2.05	0.5
Healy03	KS1	80.559	−68.926	31.86	−2.65	0.3
Healy03	KS3	80.543	−68.775	31.68	−2.82	1.0
Healy03	KS5	80.518	−68.585	31.65	−2.85	1.4
Healy03	KS7	80.487	−68.322	31.89	−2.62	0.6
Healy03	KS9	80.462	−68.039	32.02	−2.50	0.2
Healy03	KS11	80.420	−67.816	31.69	−2.82	0.9
Healy03	KS13	80.394	−67.567	32.84	−1.72	1.1
Healy03	KS15	80.371	−67.422	32.46	−2.08	1.6

Table 3. (Continued)

Cruise	Station	Latitude	Longitude	S_{HW}	$\delta^{18}O_{HW}$ (‰)	LSIM (m)
Healy03	KN7	81.144	−64.116	32.46	−2.31	1.0
Healy03	KN6	81.167	−64.297	31.89	−2.92	1.7
Healy03	KN5	81.191	−64.498	31.48	−3.36	0.5
Healy03	KN4	81.216	−64.662	31.62	−3.21	2.3
Healy03	KN3	81.240	−64.838	31.48	−3.35	0.5
Healy03	KN2	81.263	−65.020	32.34	−2.44	0.9
Healy03	KN1	81.284	−65.146	32.35	−2.43	1.4
Healy03	RN7	82.009	−60.380	31.57	−2.91	1.2
Healy03	RN6	82.025	−60.592	31.91	−2.59	0.3
Healy03	RN5	82.051	−60.794	31.78	−2.71	1.0
Healy03	RN4	82.069	−61.012	31.98	−2.52	0.8
Healy03	RN3	82.091	−61.184	31.71	−2.78	0.8
Healy03	RN2	82.111	−61.388	31.82	−2.68	0.8
Healy03	RN1	82.126	−61.611	31.69	−2.81	0.4
LSSL97	H1	61.824	−65.999	32.69	−1.48	0.0
LSSL97	H2	61.710	−65.597	32.83	−1.36	0.0
LSSL97	H3	61.292	−64.606	32.89	−1.32	0.0
LSSL97	H4	61.166	−64.585	32.55	−1.58	0.1
LSSL97	H5	61.010	−64.544	32.89	−1.32	0.2
LSSL97	H6	60.855	−64.531	33.02	−1.22	0.0
LSSL97	H7	60.731	−64.493	32.69	−1.47	0.0
LSSL97	D1	66.519	−60.799	32.94	−1.65	0.4
LSSL97	D2	66.614	−60.359	32.56	−2.03	1.0
LSSL97	D3	66.713	−59.917	32.41	−2.18	0.5
LSSL97	D4	66.834	−59.358	32.53	−2.06	1.1
LSSL97	D5	67.047	−58.254	32.85	−1.74	0.9
LSSL97	D6	67.049	−57.220	33.49	−1.11	1.4
LSSL97	D9	67.048	−54.592	33.49	−1.11	0.7
LSSL97	J1	75.837	−81.456	32.86	−1.71	0.5
LSSL97	J2	75.914	−81.379	32.55	−2.00	0.8
LSSL97	J3	75.982	−81.313	32.67	−1.89	0.9
LSSL97	J4	76.054	−81.247	33.17	−1.42	0.8
LSSL97	S1	78.401	−73.279	31.62	−2.48	0.3
LSSL97	S2	78.333	−73.661	33.19	−1.27	0.0
LSSL97	S3	78.334	−74.075	32.80	−1.57	0.0
LSSL97	S4	78.332	−74.506	32.78	−1.59	0.3
LSSL97	S5	78.334	−74.944	32.95	−1.46	0.0

contributions. Local sea ice melt fractions are calculated only for samples with salinities less than or equal to the halocline water endmember salinity for each station. Samples with larger salinities plot on or close to the halocline-Atlantic water line and are therefore presumed to be deeper water of Arctic origin that has not been affected by surface processes.

The largest sources of uncertainty in the calculation of local sea ice melt fractions stem from the estimation of the regression coefficients of the Atlantic-halocline mixing line. Variation on the estimates of the slope and/or intercept of the Atlantic-halocline mixing line result in maximum uncertainties of ± 0.03 and 1.8 meters for the local sea ice melt fractions and their associated inventories, respectively.

5. Results

For each of the stations in the CAA, Nares Strait, and Baffin Bay, we have estimated the total inventories (in meters) of PW, MW, net SIM, and local SIM in the upper ocean by vertically integrating the fractions of the various components, as derived by the methods described above. Inventories were determined at each station by first interpolating vertical profiles of these water type fractions onto a uniform grid at 5 m intervals, and then integrating between the surface and 150 meters. The integration was restricted to the depth range of highest sampling resolution which is also the region in which the majority of MW and SIM reside, although Pacific water influence extends deeper. Station inventories of each water type are plotted by section in Figures 7–16 as bar graphs aligned either horizontally for zonal sections or vertically for meridional sections. Three maps, indicating station numbers and locations for each transect, are plotted in Figure 6 for orientation.

a. 1997 sections

The lowest inventories of MW (4–5 m) were observed in eastern Davis Strait (Fig. 9), within the influence of the West Greenland Current. Smith (Fig. 7) and Jones (Fig. 8) Sounds had larger MW inventories (8–10 m), suggesting that either the western CAA provided a source of MW in addition to that entering Baffin Bay via Nares Strait during summer 1997 or the waters transiting Nares Strait were re-circulated through Jones Sound via a branch of the Baffin Current (Fissel *et al.,* 1988; Bourke *et al.,* 1989; Tang *et al.,* 2004). Western Davis Strait exhibited MW inventories similar to those found in southern Jones Sound, consistent with the southward transport of these freshwaters via the Baffin Current.

In Hudson Strait, MW inventories were higher (13–16 m) on the northern and southern edges of the strait and lower (8–9 m) in the center (Fig. 10). The southernmost station in Hudson Strait exhibited the highest MW inventory ($\sim$16 m) observed during the 1997 expedition. The inventory distributions in Figure10 indicate that meteoric waters enter Hudson Strait on the northern (inflow from Baffin Bay) side, likely via a branch of the Baffin Island Current. The MW inventories on the northern side of Hudson Strait might be slightly overestimated due to the relatively heavy $\delta^{18}O$ endmember assignment ($-14‰$) for this section. Assigning the average Arctic MW value ($-18.8‰$) results in somewhat lower MW fractions ($\sim$9 m) at these stations, in better agreement with those observed in Davis Strait (Fig. 9) and Smith and Jones sounds (Figs. 7–8). On the southern side, MW exits the strait in a narrow band likely reflecting the export of accumulated river runoff in

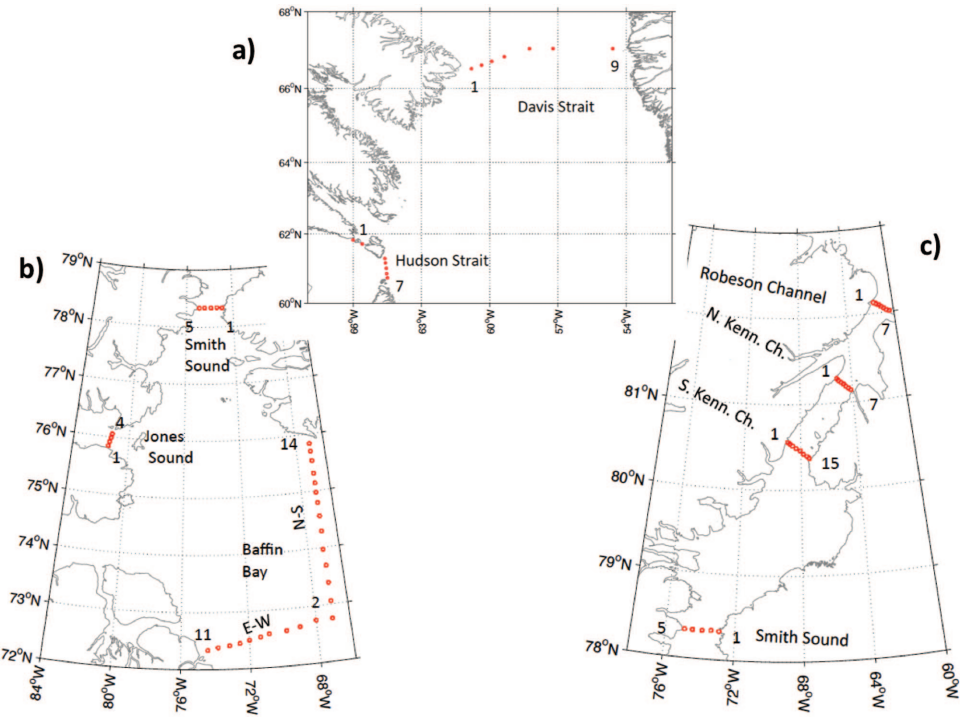

Figure 6. Maps showing the locations and stations numbers comprising transects occupied in (a) Davis and Hudson straits; (b) Smith Sound, Jones Sound, and Baffin Bay; and (c) Nares Strait.

Hudson Bay. The inventories in the Hudson Strait section are generally consistent with previous $\delta^{18}O$ distributions in Foxe Basin and Hudson Strait (Tan and Strain, 1996) and our understanding of the circulation in this strait.

Pacific water inventories were highest (>90 m) across Jones and Smith sounds (Figs. 7–8), where Arctic-origin waters enter the bay, and in western Davis Strait (Fig. 9) where they exit. Inventories were lowest (<60 m) in eastern Davis Strait, where relatively warm and saline Atlantic-origin waters enter Baffin Bay via the West Greenland Current (Tang *et al.,* 2004), and southern Hudson Strait (Fig. 10). Pacific inventories were slightly higher (~80 m) in northern Hudson Strait, presumably indicating the influence of the southward-flowing Baffin Current (Straneo and Saucier, 2008).

Inventories of brine were generally highest (i.e., had the most negative net SIM inventory) in regions where PW and MW contributions were relatively high, consistent with a predominantly Arctic-origin for this water. The largest brine contributions (≤ -8 m) were present in Jones (Fig. 8) and Smith sounds (Fig. 7) as well as western Davis Strait (Fig. 9). Smaller brine contributions (i.e., less negative inventories of net SIM) occurred in eastern Davis Strait (≥ -5 m), suggesting a lesser influence from the Arctic throughflow and/or more SIM. Net SIM inventories were slightly less negative in Hudson Strait

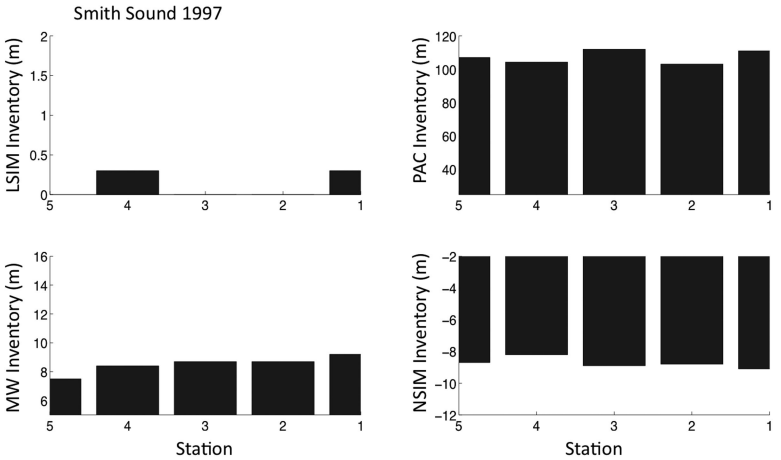

Figure 7. Bar graphs showing the inventories of local sea ice meltwater (LSIM, upper left), Pacific water (PAC, upper right), meteoric water (MW, lower left), and net sea ice meltwater (NSIM, lower right) over the top 150 meters at stations 1–5 occupied in Smith Sound, 1997. Station locations are shown on Figure 6b and are arranged on the bar graphs from west (left) to east (right).

compared to Smith and Jones sounds, indicating less Arctic influence, but were still more negative than those observed in eastern Davis Strait.

Local SIM inventories were generally very low throughout the study area, especially in Smith Sound (Fig. 7) and Hudson Strait (Fig. 10). Both Jones Sound (Fig. 8) and Davis

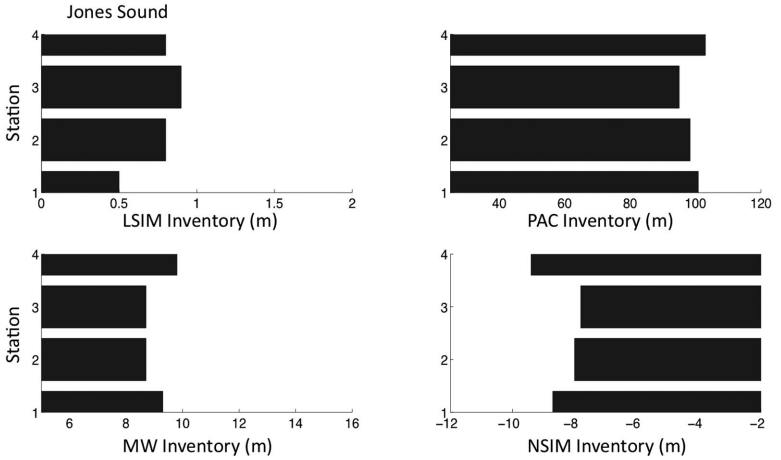

Figure 8. Bar graphs showing the inventories of local sea ice meltwater (LSIM, upper left), Pacific water (PAC, upper right), meteoric water (MW, lower left), and net sea ice meltwater (NSIM, lower right) over the top 150 meters at stations 1–4 occupied in Jones Sound, 1997. Station locations are shown on Figure 6b and are arranged on the bar graphs from south (bottom) to north (top).

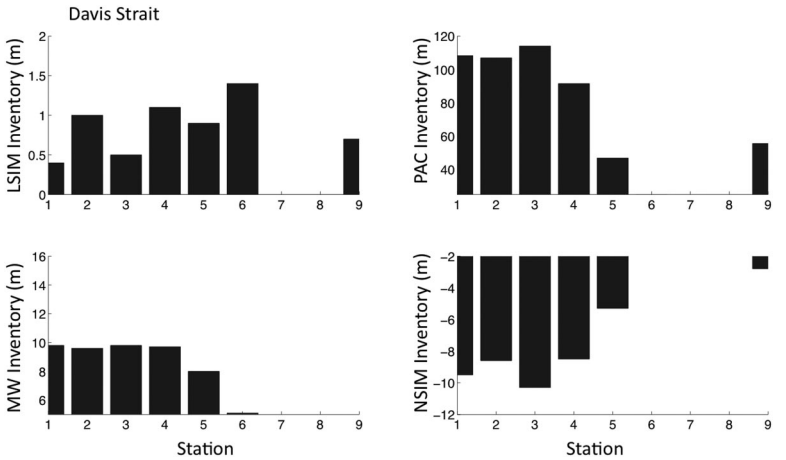

Figure 9. Bar graphs showing the inventories of local sea ice meltwater (LSIM, upper left), Pacific water (PAC, upper right), meteoric water (MW, lower left), and net sea ice meltwater (NSIM, lower right) over the top 150 meters at stations 1–9 occupied in Davis Strait, 1997. Station locations are shown on Figure 6a and are arranged on the bar graphs from west (left) to east (right).

Strait (Fig. 9) exhibited relatively large inventories of local SIM, reaching up to 1.4 m. The highest inventory (~1.4 m) was observed in eastern Davis Strait. This is not surprising as the relatively warm waters of the West Greenland Current have been known to keep eastern Davis Strait relatively ice free year around (Tang *et al.,* 2004).

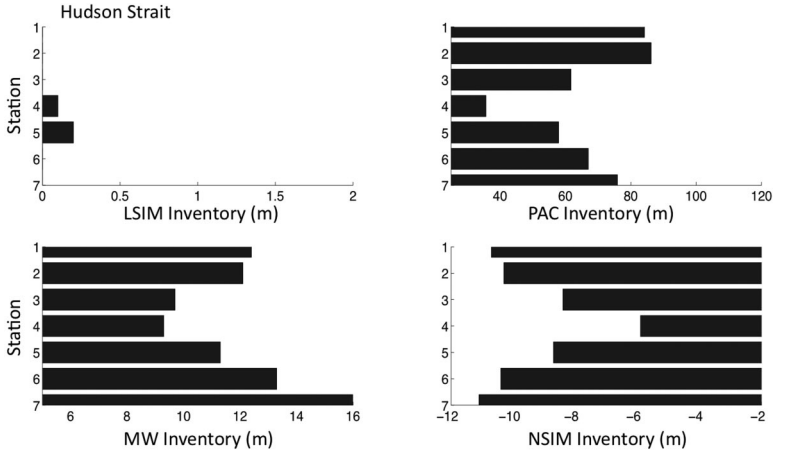

Figure 10. Bar graphs showing the inventories of local sea ice meltwater (LSIM, upper left), Pacific water (PAC, upper right), meteoric water (MW, lower left), and net sea ice meltwater (NSIM, lower right) over the top 150 meters at stations 1–7 occupied in Hudson Strait, 1997. Station locations are shown on Figure 6a and are arranged on the bar graphs from south (bottom) to north (top).

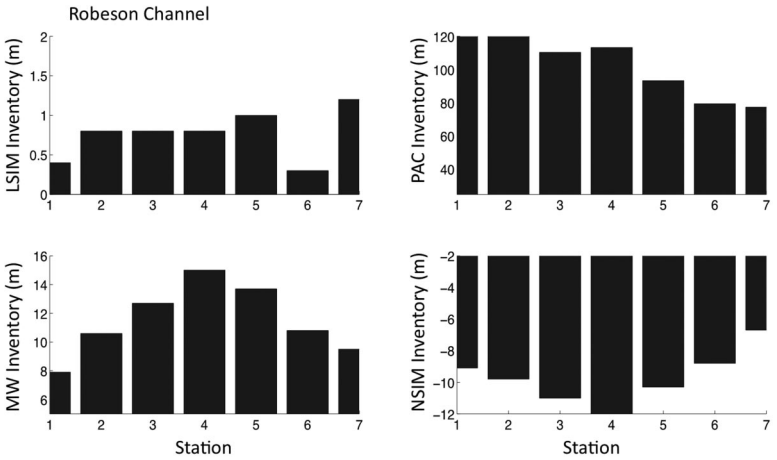

Figure 11. Bar graphs showing the inventories of local sea ice meltwater (LSIM, upper left), Pacific water (PAC, upper right), meteoric water (MW, lower left), and net sea ice meltwater (NSIM, lower right) over the top 150 meters at stations 1–7 occupied in Robeson Channel, 2003. Station locations are shown on Figure 6c and are arranged on the bar graphs from west (left) to east (right).

b. Nares Strait and Baffin Bay, 2003

Pacific water inventories decreased southward through Nares Strait, in agreement with findings by Munchow *et al.* (2007), from maxima concentrated in western Robeson Channel (Fig. 11, 80–120 m) to more diffuse, slightly lower inventories over southern Kennedy Channel (Fig. 13) and Smith Sound (Fig. 14, 50–70 m, Fig. 8b). In the eastern halves of Smith Sound and southern Kennedy Channel, the PW inventories were slightly lower (difference of ~10 m) than those in the western half. The same general pattern was observed in Baffin Bay (Figs. 15–16), as PW influence was highest in the western half and lower in the central and northern portions of the bay. However, PW inventories were higher in western Baffin Bay compared to Smith Sound and southern Kennedy Channel, consistent with a small, but significant additional input of PW from Jones and Lancaster Sounds via the western archipelago (Falkner *et al.,* in prep.). The relatively low PW inventories observed in northeast Baffin Bay and eastern Smith Sound and south Kennedy Channel were likely a consequence of Atlantic-derived waters carried northward from Davis Strait via the West Greenland Current.

Meteoric and Pacific water inventories shared similar distributions. Highest MW inventories were generally located in the Robeson and northern Kennedy Channels and decreased southward through Nares Strait (Figs. 11–14). Similarly, western Baffin Bay had higher inventories of MW (Fig. 15), but differences between the inventories in the western and northeastern bay (Fig. 16) were much smaller relative to those observed in the PW inventories.

Net SIM inventories were negative everywhere, implying a net removal of freshwater via ice formation rather than melting. Similar to the distribution of PW inventories, the

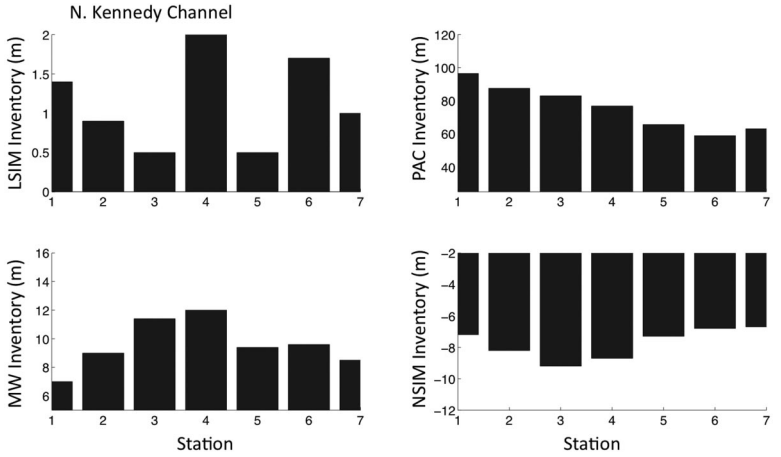

Figure 12. Bar graphs showing the inventories of local sea ice meltwater (LSIM, upper left), Pacific water (PAC, upper right), meteoric water (MW, lower left), and net sea ice meltwater (NSIM, lower right) over the top 150 meters at stations 1–7 occupied in North Kennedy Channel, 2003. Station locations are shown on Figure 6c and are arranged on the bar graphs from west (left) to east (right).

influence of brine (negative net SIM) was largest (most negative) in western Robeson Channel (Fig. 11) and decreased southward to Smith Sound (Fig. 14). Lowest brine contributions (i.e., least negative SIM) were present at the northernmost stations of Baffin

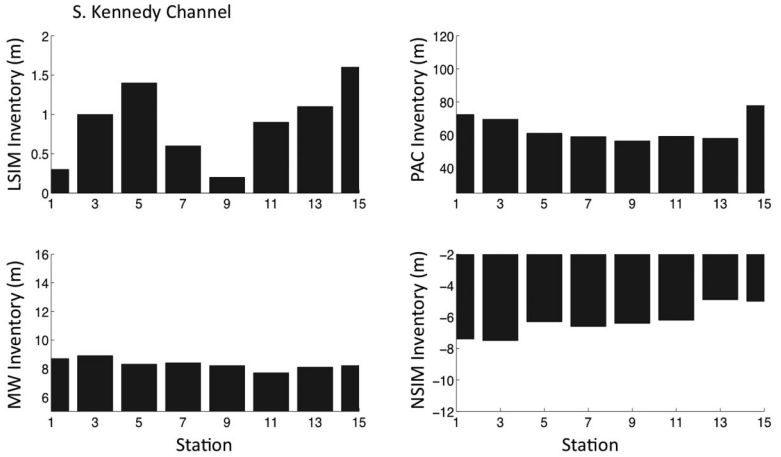

Figure 13. Bar graphs showing the inventories of local sea ice meltwater (LSIM, upper left), Pacific water (PAC, upper right), meteoric water (MW, lower left), and net sea ice meltwater (NSIM, lower right) over the top 150 meters at stations 1–15 occupied in South Kennedy Channel, 2003. Station locations are shown on Figure 6c and are arranged on the bar graphs from west (left) to east (right).

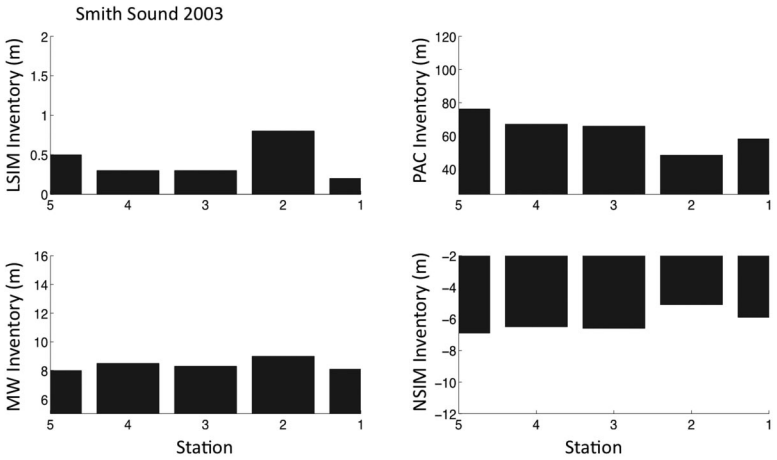

Figure 14. Bar graphs showing the inventories of local sea ice meltwater (LSIM, upper left), Pacific water (PAC, upper right), meteoric water (MW, lower left), and net sea ice meltwater (NSIM, lower right) over the top 150 meters at stations 1–5 occupied in Smith Sound, 2003. Station locations are shown on Figure 6c and are arranged on the bar graphs from west (left) to east (right).

Bay (Fig. 16) and easternmost stations of Smith Sound (Fig. 14) and southern Kennedy Channel (Fig. 13). The association of a less brine (less negative SIM) with a lower influence from Pacific water (i.e., higher influence from Atlantic water) supports the interpretation that these stations were within the stream of the West Greenland Current.

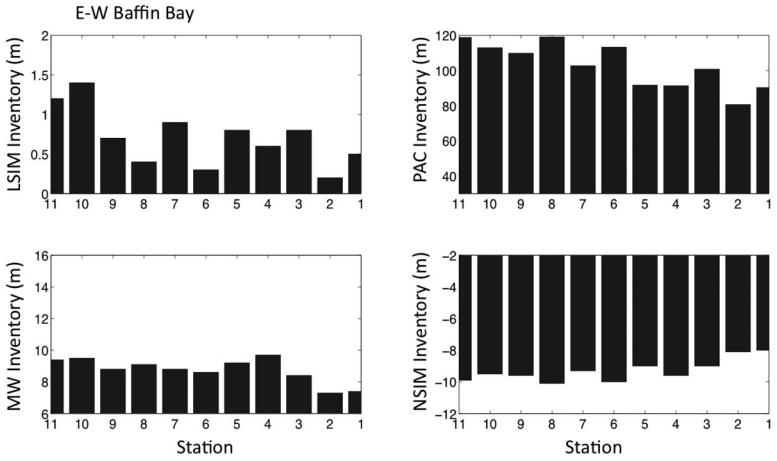

Figure 15. Bar graphs showing the inventories of local sea ice meltwater (LSIM, upper left), Pacific water (PAC, upper right), meteoric water (MW, lower left), and net sea ice meltwater (NSIM, lower right) over the top 150 meters at stations 1–11 occupied across an east-west section in Baffin Bay, 2003. Station locations are shown on Figure 6b and are arranged on the bar graphs from west (left) to east (right).

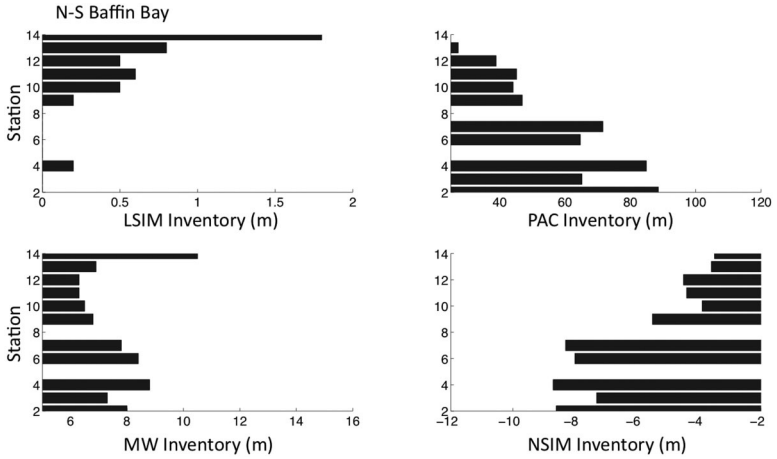

Figure 16. Bar graphs showing the inventories of local sea ice meltwater (LSIM, upper left), Pacific water (PAC, upper right), meteoric water (MW, lower left), and net sea ice meltwater (NSIM, lower right) over the top 150 meters at stations 2–14 occupied across a north-south section in Baffin Bay, 2003. Station locations are shown on Figure 6b and are arranged on the bar graphs from south (bottom) to north (top).

Local SIM inventories generally ranged between 0.2 and 1.6 m in Nares Strait, with the larger contributions ($\geq$1.0 m) concentrated in Kennedy Channel (Figs. 12–13) and the easternmost station of Robeson Channel (Fig. 11). A similar range of local SIM inventories was observed in Baffin Bay (Figs. 15–16). Inventories were highest at the northernmost and westernmost stations, associated with the West Greenland and Baffin Currents, respectively. Inventories were generally low ($\leq$0.9 m) in central Baffin Bay.

6. Discussion

a. Local sea ice meltwater contribution

Tan and Strain (1980) estimated an average sea-ice thickness of 1.5 meters for Baffin Bay based on SIM inventories, an estimate that agreed well with observed sea ice thicknesses (1.3 m). They assumed that most locally formed sea ice also melted locally. Our local SIM inventories generally agree with Tan and Strain's (1980) estimates; however, instead of a patchy distribution of meltwater influence, we find meltwater concentrated in the southward and northward flowing Baffin and West Greenland Currents, respectively. The higher inventories observed in Nares Strait, particularly northern Kennedy Channel, might be explained by the higher latitude relative to Baffin Bay, and therefore later onset of melt. Also, the geometry of the strait (relatively narrow) makes it prone to ice bridging and so it retains ice later in the melt season (Barber *et al.,* 2001).

The lack of local SIM in Hudson Strait is surprising as Hudson Bay melts all of its seasonal ice by the end of summer and transports the melt products along with runoff in a

well-defined coastal current that exits Hudson Strait on the southern side (Tan and Strain, 1996; Straneo and Saucier, 2008; Granskog *et al.,* 2009). The strong surface circulation, forced by the MW input (over 700 km^3 yr^{-1}) may have swept away SIM prior to our sampling in late summer or entrained deeper water containing brine so as to mute the seasonal SIM signal.

b. Potential impact of inherited brine on detecting glacial runoff

As melting of the Greenland Ice Sheet continues to accelerate, the contributions from glacial runoff to upper ocean waters of Nares Strait and Baffin Bay may increase. However, the influence of glacial runoff cannot be determined with any confidence by simple extrapolation of the salinity-$\delta^{18}O$ linear relationship to assess the apparent freshwater (S = 0) source. Although glacial meltwater is isotopically lighter than average Arctic meteoric water (−18.8‰), the release of brine via net sea ice formation can result in salinity-$\delta^{18}O$ relationships with highly negative intercepts that could be misinterpreted as an influence from glacial melt. Mixing lines between brine-enriched halocline water and Atlantic water yield intercepts (Table 2) similar to (if somewhat lower than) $\delta^{18}O$ values representative of glacial meltwater.

Salinity and $\delta^{18}O$ data collected next to the outflow of the Petermann Glacier (Fig. 17), with high likelihood of strong glacial meltwater influence (Johnson *et al.,* 2011), illustrate this close resemblance. Samples exhibiting influence of glacial meltwater are indistinguishable from data collected elsewhere in Nares Strait and Baffin Bay. Additional information (e.g., geochemical tracers) will be needed to distinguish between signatures of net sea ice formation and influence from glacial runoff in these regions.

c. Temporal variability in freshwater composition of Smith Sound through Nares Strait

The inventories of PW and brine (negative SIM) were ~44 and 2.5 m lower, respectively, in Smith Sound during 2003 (Fig. 14) than in 1997 (Fig. 7) and the spatial distributions changed from relatively homogenous (1997) to a west-east gradient (2003). Given the general correlation observed between these two water types in the CAA and Baffin Bay, we speculate these differences are related and result from a decrease in PW and brine entering Nares Strait from the Arctic Ocean between 1997 and 2003. In contrast, MW inventories were similar in magnitude and spatial distribution in 1997 and 2003. Assuming an Arctic origin for the meteoric water, we propose that the volumetric transport of Pacific and meteoric waters through Nares Strait are not necessarily closely coupled.

The Arctic Oscillation (AO) is defined as the principle mode of variability in the wintertime sea-level pressure over the Arctic Ocean (Thompson and Wallace, 1998). Variability in the Arctic Oscillation has been linked to shifts of the surface circulation in the Arctic Ocean (McLaughlin *et al.,* 1996; Proshutinsky and Johnson, 1997; Morison *et al.,* 1998; Steele *et al.,* 2004). For example, a positive AO index (cyclonic phase) is associated with a weakening of the anticyclonic Beaufort Gyre and a shift in the Transpolar Drift (TPD) from a rough alignment over the Lomonosov Ridge toward North America

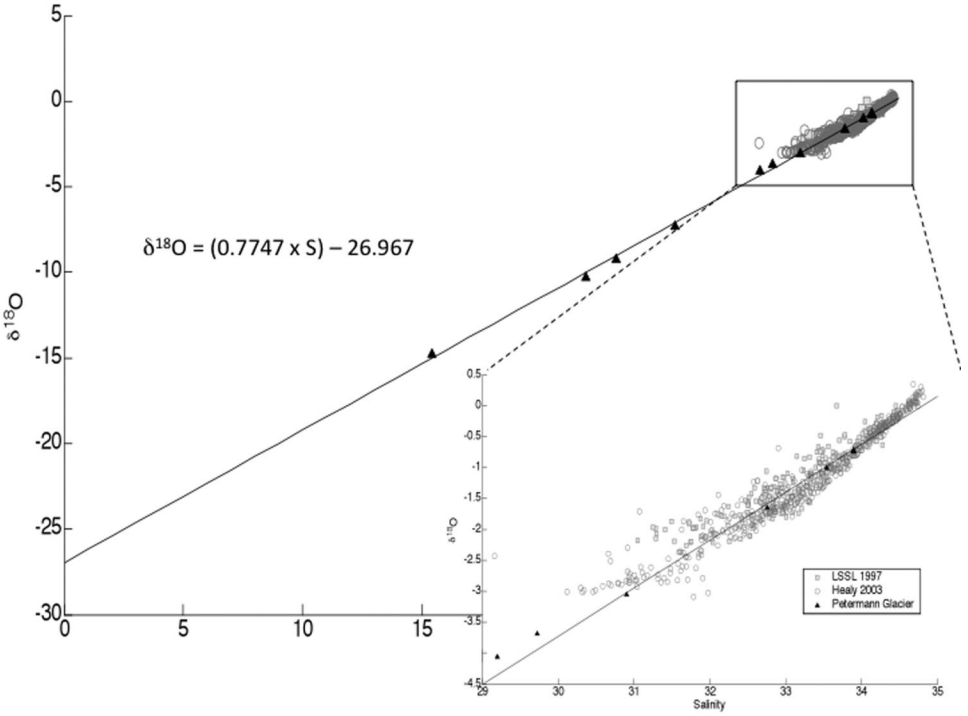

Figure 17. A comparison of salinity-$\delta^{18}O$ relationships between data collected from next to the outflow of the Petermann Glacier (black triangles) located on the Greenland side of Hall Basin versus all data collected during 1997 (dark gray squares) and 2003 (light gray circles). The inset shows a zoomed-in view between salinities 29 and 35 where all the 1997 and 2003 data plot. The black line is the least-squares linear regression ($\delta^{18}O = 0.7747*S - 26.967$; $R^2 = 0.9985$) of the Petermann Glacier data.

(McLaughlin *et al.,* 1996; Morison *et al.,* 1998). A negative (anticyclonic) AO phase is associated with an expansion of the Beaufort Gyre and an alignment of the TPD over the Lomonosov Ridge. The AO shifted to a highly positive phase in 1989–1990 and slowly returned to a more anticyclonic phase between 1995 and 2005 (Morison *et al.,* 2006).

Steele *et al.* (2004) speculated that during cyclonic (positive) AO phases, the shifted TPD could result in a separation of Pacific summer halocline waters in the outflows to the North Atlantic (western CAA and Nares and Fram straits). In contrast, anticyclonic (negative) phases would likely result in a combined flow through the western CAA and a potentially weaker Pacific water signature at Fram and Nares Straits. Observations of the temporal variability in the Pacific contribution to both Fram Strait (Jones *et al.,* 2003; Taylor *et al.,* 2003) and the East Greenland Current (Sutherland *et al.,* 2009) have supported Steele *et al.*'s hypothesis whereas at least one study (Falck *et al.,* 2005) has argued against it.

Falck *et al.* (2005) found significant contributions of Pacific water north of Fram Strait in

1984 and 1990 and suggested that such influence of Pacific water during a predominately anticyclonic period lies in contrast to the circulation scheme proposed by Steele *et al.* (2004). This is in slight contrast to the findings of Taylor *et al.* (2003), who reported a somewhat lower Pacific influence at Fram Strait in 1987 (negative AO) relative to 1998 (positive AO). By combining a set of historical sections occupied between 1984 and 2004 in the vicinity of Denmark Strait, Sutherland *et al.* (2009) found that the Pacific water contribution was significantly correlated with the AO, in support of Steele *et al.*'s hypothesis.

The observations presented in this study are two snapshots of property concentrations separated by six years and are not sufficient to determine whether or not the difference in the Pacific water concentration in Smith Sound between 1997 and 2003 is related to the relaxation of the Arctic Oscillation toward anticyclonic conditions. In addition, there are important physical processes that operate over different times scales not highly correlated with the AO. However, observations from Smith Sound (this study), Fram Strait (Jones *et al.,* 2003; Taylor *et al.,* 2003), and the East Greenland Current (Sutherland *et al.,* 2009) together indicate a reduced Pacific influence to Nares and Fram straits during the early 2000s compared to the late 1990s, in general agreement with the hypothesis of Steele *et al.* (2004).

Inter-annual variability in the circulation through Smith Sound might also explain the lower inventories and spatial gradient in PW observed in 2003 compared to 1997. Unfortunately, too few direct observations have been accumulated to address inter-annual variability in the circulation through Nares Strait and Smith Sound. Comparison of current velocity measurements collected in Smith Sound during 1997–1998 (Melling *et al.,* 2001) and August 2003 (Munchow *et al.,* 2007) indicates weaker southward flow during the former period. Assuming the PW concentration of Arctic waters flowing southward through Nares Strait was equal during both time periods, a lower contribution of PW might be expected in Smith Sound during 1997 as a consequence of the weaker southward flow; but that would run counter to our observations. The methods used in the two studies measuring currents (moorings versus continuous acoustic Doppler current profiling) resolved very different temporal and spatial scales, rendering any comparison between the two periods very uncertain.

Alternatively, modeling studies can offer some insight into the effect of circulation versus water type composition on the variability in PW inventories in Smith Sound. Jahn *et al.* (2010) incorporated passive tracers of Pacific water, Eurasian and North American river runoff, and sea ice (both liquid and solid forms) in a fully coupled general circulation model to study inter-annual variability in the export of these freshwaters through the western CAA and Fram and Nares straits. They conclude that the relative magnitude of the flux of Pacific water through Fram and Nares straits depends more on the concentration of Pacific water than the magnitude of velocity anomalies. We therefore suggest that variability observed in the composition of the waters in Smith Sound is likely the result of

changes in the Pacific water contributions advected from the Arctic Ocean through Nares Strait. Is this variability related to the Arctic Oscillation?

Jahn *et al.* (2010) argued that variability in the flux of Eurasian river runoff through Fram/Nares straits is out of phase with that of Pacific water. According to their study, variability in the fluxes of Pacific and Eurasian river runoff was better correlated with sea-level pressure variability over the central Arctic (which they represent as a "vorticity index") than with larger-scale atmospheric indices (e.g., the Arctic Oscillation; Steele *et al.,* 2004). Concentrations of Pacific water were higher at Fram/Nares straits during predominately cyclonic phases of this vorticity index because such atmospheric forcing resulted in a release of Pacific water from a weakened Beaufort Gyre (i.e., Proshutinsky *et al.,* 2002). In contrast, the flux of Eurasian river runoff increased during anticyclonic phases, in agreement with prior observational studies (Dmitrenko *et al.* 2008; Bauch *et al.,* 2009).

Assuming the meteoric water observed in Smith Sound was primarily derived from Eurasian sources, the lack of significant change in the meteoric water inventory despite the Pacific water decrease could be a consequence of this out-of-phase relationship. However, the inventory of meteoric water did not significantly increase in Smith Sound between 1997 and 2003. We cannot discount the possibility that an increased flux of Eurasian river water was concentrated at Fram Strait (instead of Nares Strait) or that an increase occurred during intervening years. Nevertheless, the reduced Pacific influence to Smith Sound observed between 1997 and 2003 is at least in general agreement with the hypothesis that the variability in the export of Pacific waters through Nares and Fram straits and the western CAA is related to atmospheric forcing upstream.

7. Conclusions

Our observations of local SIM in Baffin Bay were similar in magnitude to prior observations but, instead of a patchy distribution, meltwater was concentrated in areas influenced by major currents, suggesting ice might be rapidly advected out of Baffin Bay after the onset of melting. Similarly, the lack of local SIM in Hudson Strait could be a consequence of coastal currents carrying both runoff and meltwater out of Hudson Bay such that local contributions of SIM are undetectable by late summer.

Local sea ice meltwater is difficult to detect in large part due to relatively sparse sampling in the top 20–30 meters where the majority of SIM is found. The transition between waters influenced by SIM and underlying waters is sharp in salinity-$\delta^{18}O$ space. The calculation of local SIM fractions is sensitive to the assignment of the halocline water endmember values. Higher resolution sampling in this upper layer will significantly improve the determination of the halocline water endmember and reduce uncertainty in the local SIM calculations.

Arctic halocline water, initially brine enriched through sea ice formation over Arctic shelves, has a significant impact on the freshwater balance in regions receiving exported Arctic Ocean waters, as revealed in the salinity-$\delta^{18}O$ relationships observed there. The

presence of this exported Arctic halocline water complicates the use of salinity-$\delta^{18}O$ relationships to infer the relative influence of glacial meltwater where that might be present. Such is the case in Baffin Bay where the results presented here indicate that, however tempting, simple extrapolations of salinity-$\delta^{18}O$ relationships to a zero-salinity endmember cannot be utilized to infer significant glacial meltwater influence.

Between 1997 and 2003, a significant change in the relative contributions of Pacific water and brine (negative net SIM) was observed in the water column in Smith Sound, located in southern Nares Strait on the pathway from the Arctic Ocean to Baffin Bay. These changes are almost certainly due to changing composition at the upstream end of Nares Strait, where changes in water properties exported from the Arctic Ocean are likely to be strongly influenced by large-scale atmospheric pressure patterns and resultant forcing on upper ocean circulation. The data presented here are far too sparse in time to lend significant further credence to the sources of the observed changes; however, the significance of these changes argues strongly for increased levels of observations and modeling of the key conduits feeding freshwater from the Arctic Ocean to the headwater regions of the Atlantic meridional overturning circulation.

Acknowledgments. M. Alkire acknowledges graduate study under the NSF OPP-0634122 award to K. Falkner and R. Collier. K. Falkner acknowledges support for the field and lab work for JOIS under NSF OPP-9708420 and for CATS under NSF OPP-0230354. This work was made possible by the captains and crews of the CCGS *Louis S. St. Laurent* and USCGC *Healy* and the superb technical staff at the COAS at Oregon State University. Finally, we would also like to thank two anonymous reviewers whose comments and suggestions helped to improve this paper. Any opinions, findings, and conclusions or recommendations expressed in this material are those of the author(s) and do not necessarily reflect the views of the National Science Foundation.

REFERENCES

Aagaard, K. and E. C. Carmack. 1989. The role of sea ice and other fresh water in the Arctic circulation. J. Geophys. Res., *94,* 14485–14498.

Aksenov, Y., S. Bacon, A. C. Coward and N. P. Holliday. 2010. Polar outflow from the Arctic Ocean: A high resolution model study. J. Mar. Syst., *83,* 14–37.

Alkire, M. B., K. K. Falkner, I. Rigor, M. Steele and J. Morison. 2007. The return of Pacific waters to the upper layers of the central Arctic Ocean. Deep-Sea Res. I, *54,* 1509–1529.

Armstrong, F. A. J, C. R. Stearns and J. D. H. Strickland. 1967. The measurement of upwelling and subsequent biological processes by means of Technicon Autoanalyser and associated equipment. Deep-Sea Res., *14,* 381–389.

Azetsu-Scott, K., A. Clarke, K. Falkner, J. Hamilton, E. P. Jones, C. Lee, B. Petrie, S. Prinsenberg, M. Starr and P. Yeats. 2010. Calcium carbonate saturation states in the waters of the Canadian Arctic Archipelago and the Labrador Sea. J. Geophys. Res., *115,* doi:10.1029/2009JC005917.

Barber, D. G., J. M. Hanesiak, W. Chan and J. Piwowar. 2001. Sea-ice and meteorological conditions in northern Baffin Bay and the North Water Polynya between 1979 and 1996. Atmos. Ocean., *39,* 343–359.

Bauch, D., I. A. Dmitrenko, C. Wegner, J. Holemann, S. A. Kirillov, L. A. Timokhov and H. Kassens. 2009. Exchange of Laptev Sea and Arctic Ocean halocline waters in response to atmospheric forcing. J. Geophys. Res., *114,* doi:10.1029/2008JC005062.

Bauch, D. P. Schlosser and R. G. Fairbanks. 1995. Freshwater balance and the sources of deep and

bottom waters in the Arctic Ocean inferred from the distribution of ^{2}H and ^{18}O. Prog. Oceanogr., *35,* 53–80.

Bedard, P., C. Hillaire-Marcel and P. Page. 1981. ^{18}O modeling of freshwater inputs in Baffin Bay and Canadian Arctic coastal waters. Nature, *293,* 287–289.

Bernhardt, H. and A. Wilhelms. 1967. The continuous determination of low level iron, soluble phosphate and total phosphate with the autoanalyser. (Paper presented at Technicon Symposium.)

Bourke, R. H., V. G. Addison and R. G. Paquette. 1989. Oceanography of Nares Strait and Northern Baffin Bay in 1986 with emphasis on deep and bottom water formation. J. Geophys. Res., *94,* 8289–8302.

Cooper, L. W., J. W. McClelland, R. M. Holmes, P. A. Raymond, J. J. Gibson, C. K. Guay and B. J. Peterson. 2008. Flow-weighted values of runoff tracers (δ18O, DOC, Ba, alkalinity) from the six largest Arctic rivers. Geophys. Res. Lett., *35,* doi:10.1029/2008GL035007.

Cooper, L. W., T. E. Whitledge and J. M. Grebmeier. 1997. The nutrient, salinity, and stable oxygen isotope composition of Bering and Chukchi seas waters in and near the Bering Strait. J. Geophys. Res., *102,* 12563–12573.

Coote, A. R. and E. P. Jones. 1982. Nutrient distributions and their relationships to water masses in Baffin Bay. Can. J. Fish. Aquat. Sci., *39,* 1210–1214.

Craig, H. and L. I. Gordon. 1965. Deuterium and oxygen 18 variations in the ocean and the marine atmosphere, *in* Stable Isotopes in Oceanographic Studies and Paleotemperatures, E. Tongiorgi, ed., Consiglio Nazionale delle Ricerche, 9–130.

Dansgaard, W. and H. Tauber. 1969. Glacier oxygen 18 content and Pleistocene ocean temperatures. Science, *166,* 499–502.

Dmitrenko, I. A., S. A. Kirillov and L. B. Tremblay. 2008. The long-term and interannual variability of summer fresh water storage over the eastern Siberian shelf: implications for climatic change. J. Geophys. Res., *113,* doi:10.1029/2007JC004304.

Drinkwater, K. F. 1988. On the mean and tidal currents in Hudson Strait. Atmos. Ocean., *26,* 252–266.

Dyurgerov, M., A. Bring and G. Destouni. 2010. Integrated assessment of changes in freshwater inflow to the Arctic Ocean. J. Geophys. Res., *115,* doi:10.1029/2009JD013060.

Falck, E., G. Kattner and G. Budeus. 2005. Disappearance of Pacific water in the northwestern Fram Strait. Geophys. Res. Lett., *32,* doi:10.1029/2005GL023400.

Falkner, K. K., M. C. O'Brien, H. Melling, E. C. Carmack, F. A. McLaughlin, A. Munchow and E. P. Jones. 2011. Interannual variability of dissolved nutrients in the Canadian Archipelago and Baffin Bay with implications for freshwater flux. (in prep.)

Fissel, D. B., J. Birch, H. Melling and R. Lake. 1988. Non-tidal flows in the Northwest Passage, *in* Canadian Technical Report of Hydrography and Ocean Sciences, *98,* Institute of Ocean Sciences, Sidney, BC, Canada, 143 pp.

Gerdes, R., M. Karcher, C. Koberle and K. Fieg. 2008. Simulating the long-term variability of liquid freshwater export from the Arctic Ocean *in* Arctic-Subarctic Ocean Fluxes: Defining the Role of the Northern Seas in Climate, R. R. Dickson, J. Meincke and P. Rhines, eds., Springer, 405–425.

Gordon, L. I., J. C. Jennings, Jr., A. A. Ross and J. M. Krest. 1994. A suggested protocol for continuous flow automated analysis of seawater nutrients (phosphate, nitrate, nitrite and silicic acid), *in* the WOCE Hydrographic Program and the Joint Global Ocean Fluxes Study, WOCE Operations Manual, Vol. 3: The Observational Program, Section 3.1: WOCE Hydrographic Program, Part 3.1.3: WHP Operations and Methods, Woods Hole, MA, 52 pp.

Granskog, M. A., R. W. Macdonald, Z. Z. A. Kuzyk, S. Senneville, C. J. Mundy, D. G. Barber, G. A. Stern and F. Saucier. 2009. Coastal conduit in southwestern Hudson Bay (Canada) in summer: Rapid transit of freshwater and significant loss of colored dissolved organic matter. J. Geophys. Res., *114,* doi:10.1029/2009JC005270.

Guay, C. K., K. K Falkner, R. D. Muench, M. Mensch, M. Frank and R. Bayer. 2001. Wind-driven transport pathways for Eurasian Arctic river discharge. J. Geophys. Res., *106,* 11469–11480.

Jahn, A., L. B. Tremblay, R. Newton, M. M. Holland, L. A. Mysak and I. A. Dmitrenko. 2010. A tracer study of the Arctic Ocean's liquid freshwater export variability. J. Geophys. Res., *115,* C07015, doi:10.1029/2009JC005873.

Johnson, H. L., A. Munchow, K. K. Falkner and H. Melling. 2011. Ocean circulation and properties in Petermann Fjord, Greenland. J. Geophys. Res., *116,* doi:10.1029/2010JC006519.

Jones, E. P., L. G. Anderson and J. H. Swift. 1998. Distribution of Atlantic and Pacific waters in the upper Arctic Ocean: Implications for circulation. Geophys. Res. Lett., *25,* 765–768.

Jones, E. P. and A. R. Coote. 1980. Nutrient distributions in the Canadian Archipelago: indicators of summer water mass and flow characteristics. Can. J. Fish. Aquat. Sci., *37,* 589–599.

Jones, E. P., J. H. Swift, L. G. Anderson, M. Lipizer, G. Civitarese, K. K. Falkner, G. Kattner and F. McLaughlin. 2003. Tracing Pacific water in the North Atlantic Ocean. J. Geophys. Res., *108,* doi:10.1029/2001JC001141.

Jungclaus, J. H., H. Haak, M. Esch, E. Roeckner and J. Marotzke. 2006. Will Greenland melting halt the thermohaline circulation. Geophys. Res. Lett., *33,* doi:10.1029/2006GL026815.

Kipphut, G. W. 1990. Glacial meltwater input to the Alaska Coastal Current: Evidence from oxygen isotope measurements. J. Geophys. Res., *95,* 5177–5181.

Koerner, R. and R. D. Russell. 1979. $\delta^{18}O$ variations in snow on the Devon Island icecap, Northwest Territories, Canada. Can. J. Earth Sci., *16,* 1419–1427.

Luthcke, S. B., H. J. Zwally, W. Abdalati, D. D. Rowlands, R. D. Ray, R. S. Nerem, F. G. Lemoine, J. J. McCarthy and D. S. Chinn. 2006. Recent Greenland ice mass loss by drainage system from satellite gravity observations. Science, *314,* 1286–1289.

Macdonald, R. W. 2000. Arctic estuaries and ice: A positive-negative estuarine couple, *in* The Freshwater Budget of the Arctic Ocean, E. L. Lewis, E. P. Jones, P. Lemke, T. D. Prowse and P. Wadhams, eds., Kluwer Academic Publishers, 383–407.

Macdonald, R. W., D. W. Paton and E. C. Carmack. 1995. The freshwater budget and under-ice spreading of Mackenzie River water in the Canadian Beaufort Sea based on salinity and $^{18}O/^{16}O$ measurements in water and ice. J. Geophys. Res., *100,* 895–919.

McLaughlin, F. A., E. C. Carmack, R. W. Macdonald, and J. K. B. Bishop. 1996. Physical and geochemical properties across the Atlantic/Pacific water mass boundary in the southern Canadian Basin. J. Geophys. Res., *101 (C1),* 1183–1197.

McLaughlin, F. A., E. C. Carmack, R. W. Macdonald, H. Melling, J. H. Swift, P. A. Wheeler, B. F. Sherr and E. B. Sherr. 2004. The joint roles of Pacific and Atlantic-origin waters in the Canada Basin, 1997–1998. Deep-Sea Res. I, *51,* 107–128.

McLaughlin, F. A., E. C. Carmack, R. G. Ingram, W. J. Williams and C. Michel. 2006. Oceanography of the Northwest Passage, *in* The Sea, *14,* A. R. Robinson and K. H. Brink, Harvard University Press, Cambridge, MA, 1213–1244.

Melling, H., T. A. Agnew, K. K. Falkner, D. A. Greenberg, C. M. Lee, A. Munchow, B. Petrie, S. J. Prinsenberg, R. M. Samelson and R. A. Woodgate. 2008. Fresh-water fluxes via Pacific and Arctic outflows across the Canadian polar shelf, *in* Arctic-Subarctic Ocean Fluxes: Defining the Role of the Northern Seas in Climate, R. R. Dickson, J. Meincke and P. Rhines, eds., Springer, 193–247.

Melling, H., Y. Gratton and G. Ingram. 2001. Ocean circulation within the North Water polynya of Baffin Bay. Atmos. Ocean., *39,* 301–325.

Melling, H., R. A. Lake, D. R. Topham and D. B. Fissel. 1984. Oceanic thermal structure in the western Canadian Arctic. Cont. Shelf Res., *3,* 233–258.

Morison, J., M. Steele and R. Andersen. 1998. Hydrography of the upper Arctic Ocean measured from the nuclear submarine U.S.S. *Pargo.* Deep-Sea Res. I, *45,* 15–38.

Morison, J., M. Steele, T. Kikuchi, K. Falkner and W. Smethie. 2006. The relaxation of central Arctic Ocean hydrography to pre-1990s climatology. Geophys. Res. Lett., *33,* doi:10.1029/2006GL026826.

Muench, R. D. 1971. The physical oceanography of the northern Baffin Bay region, Ph.D. thesis, University of Washington, Seattle.

Munchow, A., K. K. Falknerand H. Melling. 2007. Spatial continuity of measured seawater and tracer fluxes through Nares Strait, a dynamically wide channel bordering the Canadian Archipelago. J. Mar. Res., *65,* 759–788.

Myers, P. G. 2005. Impact of freshwater from the Canadian Arctic Archipelago on Labrador Sea water formation. Geophys. Res. Lett., *32,* doi:10.1029/2004GL022082.

Ostlund, H. G. and G. Hut. 1984. Arctic Ocean water mass balance from isotope data. J. Geophys. Res., *89,* 6373–6381.

Paren, J. G. and J. R. Potter. 1984. Isotopic tracers in polar seas and glacier ice. J. Geophys. Res., *89,* 749–750.

Pfirman, S., W. Haxby, H. Eicken, M. Jeffries and D. Bauch. 2004. Drifting Arctic Sea ice archives changes in surface ocean conditions. Geophys. Res. Lett., *31,* doi:10.1029/2004GL020666.

Prinsenberg, S. J. and J. Hamilton. 2005. Monitoring the volume, freshwater and heat fluxes passing through Lancaster Sound in the Canadian Arctic archipelago. Atmos. Ocean., *43,* 1–22.

Proshutinsky, A., R. H. Bourke and F. A. McLaughlin. 2002. The role of the Beaufort Gyre in Arctic climate variability: seasonal to decadal climate scales. Geophys. Res. Lett., *29,* doi:10.1029/2002GL015847.

Proshutinsky, A. Y. and M. A. Johnson. 1997. Two circulation regimes of the wind-driven Arctic Ocean. J. Geophys. Res., *102,* 12493–12514.

Redfield, A. C. and I. Friedman. 1969. The effect of meteoric water, melt water and brine on the composition of Polar Sea water and of the deep waters of the ocean. Deep-Sea Res., *16* (Suppl.), 197–224.

Rignot, E., J. E. Box, E. Burgess and E. Hanna. 2008. Mass balance of the Greenland ice sheet from 1958–2007. Geophys. Res. Lett., *35,* doi:10.1029/2008GL035417.

Rigor, I. G. and J. M. Wallace. 2004. Variations in the age of Arctic sea-ice and summer sea-ice extent. Geophys. Res. Lett., *31,* doi:10.1029/2004GL019492.

Rudels, B. 1986. The outflow of polar water through the Arctic Archipelago and the oceanographic conditions in Baffin Bay. Polar Res., *4,* 161–180.

Schlosser, P., D. Bauch, R. Fairbanks and G. Boenisch. 1994. River-runoff: mean residence time on the shelves and in the halocline. Deep-Sea Res. I, *41,* 1053–1068.

Schmidt, G. A., G. R. Bigg and E. J. Rohling. 1999. Global Seawater Oxygen-18 Database. http:data.giss.nasa.gov/o18data/.

Serreze, M. C., A. P. Barrett, A. G. Slater, R. A. Woodgate, K. Aagaard, R. B. Lammers, M. Steele, R. Moritz, M. Meredith and C. M. Lee. 2006. The large-scale freshwater cycle of the Arctic. J. Geophys. Res., *111,* doi:10.1029/2005JC003424.

Shadwick, E. H., H. Thomas, Y. Gratton, D. Leong, S. A. Moore, T. Papakyriakou and A. E. F. Prowe. 2011. Export of Pacific carbon through the Arctic Archipelago to the North Atlantic. Cont. Shelf Res., *31,* 806–816.

Steele, M. and T. Boyd. 1998. Retreat of the cold halocline layer in the Arctic Ocean. J. Geophys. Res., *103,* 10419–10435.

Steele, M. and W. Ermold. 2007. Steric sea level change in the northern seas. J. Climate, *19,* 403–417.

Steele, M., J. Morison, W. Ermold, I. Rigor, M. Ortmeyer and K. Shimada. 2004. Circulation of summer Pacific halocline water in the Arctic Ocean. J. Geophys. Res., *109,* doi:10.1029/2003JC002009.

Steinacher, M., F. Joos, T. L. Frolicher, G. K. Plattner and S. C. Doney. 2009. Imminent ocean

acidification in the Arctic projected with the NCAR global coupled carbon cycle-climate model. Biogeosciences, *6,* 515–533.

Stouffer, R. J., J. Yin, J. M. Gregory, K. W. Dixon, M. J. Spelman, W. Hurlin, A. J. Weaver, M. Eby, G. M. Flato, H. Hasumi, A. Hu, J. H. Jungclaus, I. V. Kamenkovich, A. Levermann, M. Montoya, S. Murakami, S. Nawrath, A. Oka, W. R. Peltier, D. Y. Robitaille, A. Sokolov, G. Vettoretti and S. L. Weber. 2006. Investigating the causes of the response of the thermohaline circulation to past and future climate changes. J. Climate, *19,* 1365–1387.

Strain, P. M. and F. C. Tan. 1993. Seasonal evolution of oxygen isotope-salinity relationships in high-latitude surface waters. J. Geophys. Res., *98,* 14589–14598.

Straneo, F. and F. Saucier. 2008. The outflow from Hudson Strait into the Labrador Sea. Deep-Sea Res. I, *55,* 926–946.

Sutherland, D. A., R. S. Pickart, E. P. Jones, K. Azetsu-Scott, A. J. Eert and J. Olafsson. 2009. Freshwater composition of the waters off southeast Greenland and their link to the Arctic Ocean. J. Geophys. Res., *114,* doi:10.1029/2008JC004808.

Tan, F. C. and P. M. Strain. 1980. The distribution of sea ice meltwater in the Eastern Canadian Arctic. J. Geophys. Res., *85,* 1925–1932.

—— 1996. Sea ice and oxygen isotopes in Foxe Basin, Hudson Bay, and Hudson Strait, Canada. J. Geophys. Res., *101,* 20869–20876.

Tang, C. C. L., C. K. Ross, T. Yao, B. Petrie, B. M. DeTracey and E. Dunlap. 2004. The circulation, water masses and sea-ice of Baffin Bay. Prog. Oceanogr., *63,* 183–228.

Taylor, J. R., K. K Falkner, U. Schauer and M. Meredith. 2003. Quantitative considerations of dissolved barium as a tracer in the Arctic Ocean. J. Geophys. Res., *108,* doi:10.1029/2002JC001635.

Thompson, D. W. J. and J. M. Wallace. 1998. The Arctic Oscillation signature in the wintertime geopotential height and temperature fields. Geophys. Res. Lett., *25,* 1297–1300.

Velicogna, I. 2009. Increasing rates of ice mass loss from the Greenland and Antarctic ice sheets revealed by GRACE. Geophys. Res. Lett., *36,* doi:10.1029/2009GL040222.

Wallace, D. W. R. 1985. A study of the ventilation of Arctic waters using chlorofluoromethanes as tracers, Ph.D. thesis, Dalhousie, Halifax, Nova Scotia, Canada, 225 pp.

Weeks, W. F. and S. F. Ackley. 1986. The growth, structure and properties of sea ice, *in* The Geophysics of Sea Ice, N. Untersteiner, ed., Plenum Press, 9–164.

Yamamoto-Kawai, M., F. A. McLaughlin, E. C. Carmack, S. Nishino and K. Shimada. 2008. Freshwater budgets of the Canada Basin, Arctic Ocean, from salinity, $\delta^{18}O$, and nutrients. J. Geophys. Res., *113,* doi:10.1029/2006JC003858.

Yamamoto-Kawai, M., F. A. McLaughlin, E. C. Carmack, S. Nishino, K. Shimada and N. Kurita. 2009. Surface freshening of the Canada Basin, 2003–2007: river runoff versus sea ice meltwater. J. Geophys. Res., *114,* doi:10.1029/2008JC005000.

Yamamoto-Kawai, M., N. Tanaka and S. Pivovarov. 2005. Freshwater and brine behaviors in the Arctic Ocean deduced from historical data of $\delta^{18}O$ and alkalinity (1929–2002 A.D.). J. Geophys. Res., *110,* doi:10.1029/2004JC002793.

Received: *29 July, 2010;* revised: *20 March, 2011.*